Simultaneous analyses of fluorescence decay and anisotropy decay in green fluorescent protein dimer from jellyfish Clytia gregaria : FRET and molecular dynamics simulation

Journal of Photochemistry and Photobiology. A, Chemistry

Nunthaboot, Nadtanet; Tanaka, Fumio; Borst, Jan W.; Visser, Antonie J.W.G.

https://doi.org/10.1016/j.jphotochem.2021.113584

Journal of Photochemistry & Photobiology, A: Chemistry 423 (2022) 113584

Contents lists available at ScienceDirect

Journal of Photochemistry & Photobiology, A: Chemistry

journal homepage: www.elsevier.com/locate/jphotochem

Simultaneous analyses of fluorescence decay and anisotropy decay in green fluorescent protein dimer from jellyfish *Clytia gregaria*: FRET and molecular dynamics simulation

Nadtanet Nunthaboot [a,*], Fumio Tanaka [b,*], Jan W. Borst [c], Antonie J.W.G. Visser [c]

[a] Department of Chemistry and Center of Excellence for Innovation in Chemistry, Faculty of Science, Mahasarakham University, Mahasarakham 44150, Thailand
[b] Division of Laser Biochemistry, Institute for Laser Technology, Osaka 550-0004, Japan
[c] Laboratory of Biochemistry, Microspectroscopy Research Facility, Wageningen University and Research, P.O. Box 8128, 6700 ET Wageningen, The Netherlands

ARTICLE INFO

Keywords:
Clytia gregaria
Green fluorescence protein
Förster type resonance energy transfer
FRET
Fluorescence decay

ABSTRACT

Structural and dynamic behaviors of the green fluorescent protein dimer from jellyfish Clytia gregaria (cgGFP) were investigated by means of molecular dynamics (MD) simulation. Both neutral and ionic forms of the chromophore, p-hydroxybenzylideneimidazolinone (GYS) were considered. The partial atomic charges of the chromophore were derived by BCC and RESP approaches. The structures were compared between the anionic and neutral cgGFP, and between the two subunits (Sub A and Sub B) of the protein dimer. The observed fluorescence intensity and anisotropy decays were further analyzed with theoretical expressions by employing the atomic coordinates of neutral cgGFP obtained by MD simulation. It was assumed that the fluorescence quenching of GYSA and GYSB is ascribed to HB formations between heteroatoms of GYSs and nearby amino acids. Excellent agreement between the observed and calculated intensity decays, and the observed and calculated anisotropy decays were obtained with RESP1 model. The agreements were better in RESP model than those in BCC one. Mean quenching constants of GYSA and GYSB were 0.27 and 0.59 ns^{-1} overall MD snapshots with RESP1. Mean value of square of direction cosine between the two transition moments of GYSs was 0.74, and that of square of orientation factor was 0.53, and the FRET rates from GYSA to GYSB, and from GYSB to GYSA were 0.87 and 1.87 ns^{-1}.

1. Introduction

The green fluorescent protein (GFP) is composed of 238 amino acid residues (26.9 kDa), and displays bright green fluorescence upon excitation by blue to ultraviolet light. GFP was first isolated from jellyfish Aequorea victoria (avGFP) by Shimomura et al. [1,2]. GFP has been an excellent tool in molecular and cellular biological studies [3,4]. The crystal structures of GFP were reported by Ormö et al. for the S65T mutant [5] and by Yang et al. for wild type GFP in 1996 [6].

A number of computational works have reported on the structure of avGFP and its variants in solution by means of molecular dynamics (MD) simulation. The avGFP displays two absorption maxima at 395 nm (State A) and 475 nm (State B), which are considered to be neutral and anionic forms of the chromophore of p-hydroxybenzylideneimidazolinone (GYS) [3], respectively, in the protein. Time-resolved fluorescence study displayed additional state (State I), which is considered to be proton dissociated state of GYS in the excited state of State A [7,8]. Lill and Helms [9] have demonstrated by means of a special MD method that electronic excitation of neutral GYS in avGFP induces excited-state proton transfer to a nearby glutamic acid residue via a water molecule and a serine residue in the time domain of several tens of femtoseconds [9]. Patnaik et al. studied by MD simulation on the conformational rearrangement induced by deprotonation of GYS, as well as the associated changes in the hydrogen-bonding (HB) network, and found that the conformation near Thr203 is modified due to deprotonation [10]. Although GFP is highly fluorescent, denatured-GFP is non-fluorescent [10]. The environment of the protein likely plays an important role in its fluorescence behavior. In addition to the MD studies, quantum mechanics/molecular mechanics (QM/MM) with ONIOM calculations were carried out to investigate the effect of the β sheet on the internal rotation in the chromophore. Nifosi and Tozzini studied the solution structures of F64L, S65T, and T203Y mutated avGFP [11]. Patnaik et al., studied the

* Corresponding authors.
E-mail addresses: nadtanet.n@msu.ac.th (N. Nunthaboot), fumio.tanaka@yahoo.com (F. Tanaka).

https://doi.org/10.1016/j.jphotochem.2021.113584
Received 26 April 2021; Received in revised form 19 September 2021; Accepted 29 September 2021
Available online 16 October 2021

relationship between molecular structures and redshift in absorption spectra of S65G and S65T avGFP utilizing both MD simulation and QM/MM method [12]. An anionic form was suggested to be predominantly detected in solution for both S65G and S65T variants. Lau et al. applied MD simulation technique to investigate the effect of the very high surface charges on the structure, dynamics, and solvation shell for mutated avGFPs with a wide range of surface charges [13]. Megley et al. argued by means of quantum mechanical study and MD simulation on relationship between fluorescence quantum yields and dihedral rotations around single bonds connecting two aromatic rings of GYS in green, yellow, and blue fluorescent proteins in the excited states, and concluded that the quantum yield increases with decreasing the rotational freedom [14].

The jellyfish *Clytia gregaria* (syn. Phialidium gregarium) has GFP (cgGFP) with MW 21 kDa, isolated from extracts of *A. Victoria* [15]. Recently, cDNA for the cgGFP has been cloned, expressed in *Escherichia coli* cells, purified, and characterized [16]. The recombinant cgGFP emits a blue bioluminescence upon addition of Ca^{2+}. Crystal structure of cgGFP was determined by Titushin et al. [17]. The representative structure of cgGFP is shown in Fig. 1, in which amino acids of potential proton donor or acceptors to GYS are indicated. Although the amino acid sequence of cgGFP is homologous by only 42% with one of avGFP, their overall crystal structures display a very high degree of homology. The cgGFP displays a dimer at relatively high concentrations in solution while avGFP is monomer.

Fluorescence dynamics of cgGFP has been investigated by means of a mode-locked laser pumped with a continuous wave laser for excitation and time-correlated single-photon counting by Malikova et al. [18]. The fluorescence intensity decayed with a two-exponential function depending on the concentration. At higher concentrations, the intensity decayed with a single exponential function with the lifetime of 2.78 ns upon excitation at 470 nm and emission at 512 nm. The anisotropy decay was fitted with a double exponential decay function with correlation times of 0.64 (amplitude, 0.049) and 34.0 ns (0.300). The shorter correlation time is due to Förster type resonance energy transfer (FRET) between GYS in subunit A (GYSA) and GYS in subunit B (GYSB). The longer correlation time is due to rotational motion of the entire cgGFP protein [18].

FRET phenomena in GFP dimer have been also reported in yellow fluorescent protein (YFP; T203Y, Thr203 is replaced by Tyr in avGFP) by Shi et al. [19], and in enhanced GFP (EGFP; F64L / S65T, Phe64 and Ser65 in avGFP are replaced by Leu and Thr, respectively) by Teijeiro-Gonzalez et al. [20], where the two GFPs are connected with 15 amino acids.

Ichie and Karplus were the first who provided theoretical expressions of dynamic depolarization due to internal motions of tryptophane residues in protein, using MD structures [21]. They introduced auto-correlation function between transition moments of absorption and emission of small molecules in protein, in order to obtain time-dependent anisotropy. Henry and Hochstrasser applied MD method to determine experimental depolarization caused by FRET between the tryptophans present in myoglobin [22]. Nunthaboot et al. [23] performed MD simulation on time resolved fluorescence anisotropy decays of apoflavodoxin in which three trypthophans are present, using experimental data reported by Visser et al. [24]. The obtained results supported a model of two unidirectional FRET pathways among the tryptophans. Teijeiro-Gonzalez et al. [20] have analyzed the experimental depolarization due to FRET in homo-dimer of EGFP, by means of auto-correlation functions with the MD structures up to 500 ns.

In the present study, the experimental data on the intensity and anisotropy decays reported by Malikova et al. [18] were simultaneously analyzed with a theory of time-dependent photo-selection [25], and the MD structures of cgGFP. The MD calculations were performed for two forms of cgGFP, which contain neutral and anionic states of GYS. Effect of atomic charges on the dynamic MD structures was also examined with two models (BCC and RESP) of atomic charges of the proteins.

2. Method of computation

2.1. MD calculation

The starting structure of the dimeric form of the green fluorescent protein from *Clytia gregaria* was obtained from protein data bank with PDB entry code 2HPW [17]. In this crystallographic cell, the protein is a

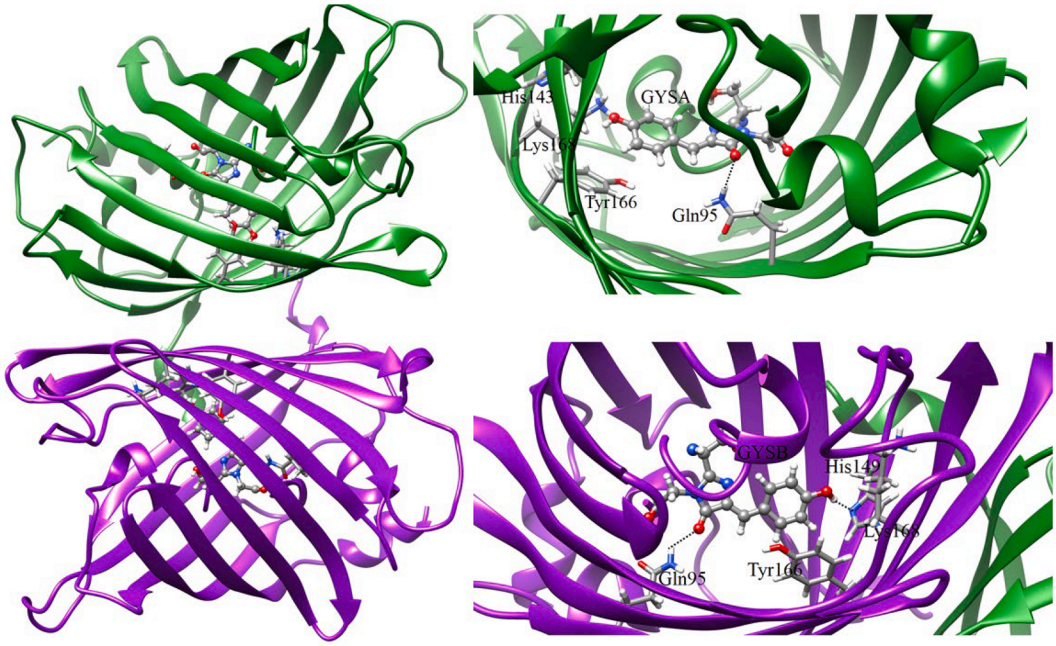

Fig. 1. Snapshot of the cgGFP. The structure was prepared with a snapshot obtained by neutral RESP1 model using Chimera software. The chromophores (GYSA in Subunit A (Sub A) , and GYSB in Subunit B (Sub B)) are represented in ball and stick model. The main H-bond pairs forming between amino acids and the two chromophores are displayed in dot lines.

monomer, so symmetry was applied to obtain the structure of the dimer. Therefore, both monomers are identical in the orientation of all side chains, chromophores, and so on. In order to investigate the effect of different protonation states of GYS, both neutral and anionic forms are assigned. In the anionic form, OH group of the phenol in GYS is deprotonated. To determine the influence of all atomic charges of chromophore, two methodologies were utilized. First, the chromophore partial atomic charges were calculated using the semi-empirical AM1-BCC charge model (BCC) implemented in Antechamber. In another model, its electrostatic potential charge was preliminary calculated using Gaussian03 at the HF/6-31G* level of theory (G03) [26]. Then the charge fitting by the restrained electrostatic potential method [27] with the Antechamber module of AMBER was utilized. The general AMBER force field [28] was used as parameters for chromophore while the FF14SB [29] was employed to treat protein structure.

All missing hydrogen atoms were added using the Leap module of the AMBER14 suit of programs [30]. Then 16$Na^{\pm}$ counter ions were added to maintain the electro-neutrality of the simulated system. To remove bad contacts, all added hydrogen atoms were preliminary minimized with 1,000 steps of steepest descents (SD) and 4000 steps of conjugated gradient (CG). The resulting protein–ligand complex was further immersed in a cubic box of pre-equilibrated TIP3P [31] water molecules with at least 12 Å distance around the complex, with the crystal structural water molecules within 10 Å from chromophore are remained. This yields simulation box containing about 17,900 water molecules with initial dimension of about 86 Å × 109 Å × 77 Å.

Before the production phase, many steps of energy minimization and equilibration protocol were utilized as follows: *(i)* 1000 steps SD and 4000 steps CG minimizations of the added water molecules; *(ii)* 1000 steps SD and 4000 steps CG minimizations of the entire system (protein, ligand, counter ions, and water molecules); *(iii)* heating the system gradually from 0 K to 298 K for 100 ps with applying a harmonic restraint weight of 100.0 kcal/(mol$Å^2$) for solute atoms; *(iv)* performing four additional MD equilibrations of each 100 ps with a decreased restraint weights from 50.0, to 25.0, to 10.0, to 5.0 kcal/(mol$Å^2$), respectively, at constant temperature of 298 K; and (*v*) consequently conducting MD simulations at a constant temperature of 298 K up to 100 ns without any restraint.

Energy minimization and MD calculations were carried out using the SANDER module of the AMBER14 software package [30]. The system was set up under the periodic boundary condition in the isobaric-isothermal ensemble (NPT) with a constant pressure of 1 atm and temperature at 298 K. The long-range electrostatic interaction was calculated based on the Particle Mesh Ewald method [32]. All bonds involving hydrogen atoms were constrained according to the SHAKE algorithm [33]. A cutoff distance of 10 Å for non-bonded pair interaction was used with an integration time step of 2 fs. Snapshots were collected every 4 ps and only the data taken from the simulation time of 60 ns to 100 ns was collected for analysis.

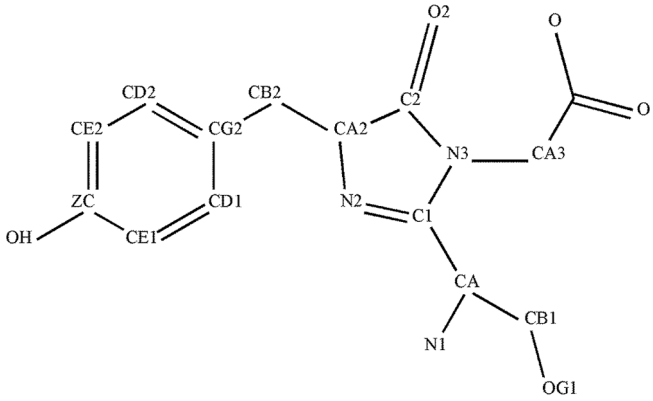

Chart 1. Atom notations of GYS.

2.2. Calculations of hydrogen-bonding distance

Steady hydrogen-bonding (HB) distances (RH) between heteroatoms (N2, O2, OH, see Chart 1) in GYS and nearby amino acids were calculated with a module of Amber 14 [30]. In many atom pairs, RH values were quite short within HB interaction radii for substantial period of MD time, though mean RH values were quite long, which is called dynamic HB here. Dynamics of RH were calculated in the following procedure;

RH between the heteroatoms in GYS and all amino acids (N and O atoms in peptide and side-chains) were calculated for all snapshots. The atom pairs were selected when the RH value displays within 0.35 nm in any snapshots.

2.3. Method of analyses

2.3.1. Fluorescence decay

When GYSA and GYSB interact by FRET, and further quenching rates of GYSA and GYSB are not the same due to non-equivalent HB structures near the chromophores, the fluorescence decay function at definite MD time, $t^{'}$, is expressed by Eq. (1) [25].

$$F(t,t^{'}) = F_1 exp\{-\lambda_1(t^{'})t\} + F_2 exp\{-\lambda_2(t^{'})t\} \quad (1)$$

Here $\lambda_1(t^{'})$ and $\lambda_2(t^{'})$ are coupling rates and are obtained by Eqs. (2) and (3) at MD time $t^{'}$.

$$\lambda_1(t^{'}) = \frac{1}{2}\left[\{k_A(t^{'}) + k_B(t^{'}) + k_{AB}(t^{'}) + k_{BA}(t^{'})\} - \sqrt{\{k_A(t^{'}) - k_B(t^{'}) + k_{AB}(t^{'}) - k_{BA}(t^{'})\}^2 + 4k_{AB}(t^{'})k_{BA}(t^{'})}\right] \quad (2)$$

$$\lambda_2(t^{'}) = \frac{1}{2}\left[\{k_A(t^{'}) + k_B(t^{'}) + k_{AB}(t^{'}) + k_{BA}(t^{'})\} + \sqrt{\{k_A(t^{'}) - k_B(t^{'}) + k_{AB}(t^{'}) - k_{BA}(t^{'})\}^2 + 4k_{AB}(t^{'})k_{BA}(t^{'})}\right] \quad (3)$$

In Eqs. (2) and (3) $k_A(t^{'})$ and $k_B(t^{'})$ are rates of GYSA and GYSB fluorescence in the absence of FRET interaction. $k_{AB}(t^{'})$ and $k_{BA}(t^{'})$ are FRET rates from GYSA to GYSB, and from GYSB to GYSA, respectively, as shown by Eqs. (4) and (5) [34,35].

$$k_{AB}(t') = k_A(t')\kappa(t')^2\left\{\frac{R_e}{R(t')}\right\}^6 \quad (4)$$

$$k_{BA}(t') = k_B(t')\kappa(t')^2\left\{\frac{R_e}{R(t')}\right\}^6 \quad (5)$$

The kappa orientation factor (κ) between transition moments of GYSA and GYSB is expressed by Eq. (6).

$$\kappa(t') = cos\theta_T(t') - 3cos\theta_A(t')cos\theta_B(t') \quad (6)$$

Here $\theta_T(t')$ is angle between directions of transition moments of GYSA and GYSB at MD time t'. Recently, VanDerMeer discusses on the property of the orientation factor kappa [36]. The direction of the transition moment in the chromophore was taken from the work by Malikova et al. [18]. The $\theta_A(t')$ is an angle between direction of the transition moment of GYSA and a distance vector connecting molecular centers of GYSA and GYSB, and $\theta_B(t')$ angle between the direction of transition moment of GYSB and the distance vector. Critical FRET distance (R_0) is given by Eqs. (7) and (8).

$$R_0(t')^6 = \kappa(t')^2R_e^6 \quad (7)$$

$$R_e^6 = \frac{Q_0 9(ln10)J}{128\pi^5 n^4 N_A} \quad (8)$$

In Eq. (8) Q_0 is the fluorescence quantum yield of GYS without FRET acceptor, n refraction index of medium, N_A Avogadro number, J overlap integral between donor absorption and acceptor emission spectra. In the present work, the absorption spectra are similar between the donor and acceptor, and so for the emission spectra. The absorption and emission spectra of cgGFP is shown in the previous work by Markowa et al. [16]. $R(t')$ is FRET donor–acceptor distance. The values of $R(t')$ was calculated between mean atomic coordinate over all aromatic atoms in GYSA and mean atomic coordinate over all aromatic atoms in GYSB at MD time of t'.

2.3.2. Method of simultaneous analyses of intensity and anisotropy decays.

GYS contains heteroatoms of N2, O2 and OH (see Chart 1), which could form hydrogen bonds (HBs) with nearby N or O atoms in amino acids. The formations of HB between GYS and nearby amino acids could influence fluorescence quenching of GYSs [37–41]. The HB structures are not equivalent between Sub A and Sub B, as demonstrated above. We assumed that the rates, $k_A(t')$ and $k_B(t')$ are expressed by Eqs. (9) and (10).

$$k_A(t') = \sum_{i=1}^{n} k_{QA}^i exp\{-C_A RH_A^i(t')\} \quad (9)$$

$$k_B(t') = \sum_{i=1}^{m} k_{QB}^i exp\{-C_B RH_B^i(t')\} \quad (10)$$

Here k_{QA}^i and k_{QB}^i quenching constants in ns^{-1} due to HB formation between a heteroatom in GYSA and nearby amino acid, and between heteroatoms in GYSB and nearby amino acid, respectively. $RH_A^i(t')$ and $RH_B^i(t')$ are HB distance in nm unit of a pair i in Sub A and in Sub B and were assumed to be all unity. When the coefficients, C_A and C_B in unit of nm^{-1} were changed from 1 to 2, the quenching rates did not show any changes. Effects of C_A and C_B on the quenching rates are considered to be included in k_{QA}^i and k_{QB}^i in Eqs. (9) and (10). Accordingly, these coefficients were set to be 1. The n and m are number of HB pairs.

Anisotropy decay is obtained by Eq. (11) [25].

$$A(t,t') = A_0\left[3cos^2\theta_T(t') + 1 + 3\{1 - cos^2\theta_T(t')\}exp\{-(k_{AB}(t') + k_{BA}(t'))t\}\right]exp(-t/\phi) \quad (11)$$

Here $\theta_T(t')$ is an angle between transition moments of GYSA and GYSB, and ϕ is rotational correlation time of entire protein (ϕ=34 ns) [18]. A_0 Is a normalization constant.

Calculated fluorescence decay and anisotropy decay are obtained by Eqs. (12) and (13).

$$F_{cal}(t) = \langle F(t,t')\rangle_{AV} \quad (12)$$

$$A_{cal}(t) = \langle A(t,t')\rangle_{AV} \quad (13)$$

Here $\langle....\rangle_{AV}$ indicates averaging procedure over all snapshots with MD time t' (10,000 snapshots with 4 ps intervals).

The values of k_{QA}^i (i = 1 to n) and k_{QB}^i (i = 1 to m), R_e, F_1, F_2 and A_0 were determined so as to obtain minimum values of total chi square χ_T^2 given by Eq. (14), according to Marquardt algorithm.

$$\chi_T^2 = \frac{1}{2}\{\chi_F^2 + \chi_A^2\} \quad (14)$$

$$\chi_F^2 = \frac{1}{n_F}\sum_{j=1}^{n_F}\left[\frac{\{F_{cal}(t_j) - F_{obs}(t_j)\}^2}{F_{cal}(t_j)}\right] \quad (15)$$

$$\chi_A^2 = \frac{1}{n_F}\sum_{j=1}^{n_F}\left[\frac{\{A_{cal}(t_j) - A_{obs}(t_j)\}^2}{A_{cal}(t_j)}\right] \quad (16)$$

n_F is number of decay time t_j (500 with 0.04 ns intervals). The values of chi squares for intensity and anisotropy were obtained by Eqs. (15) and (16). Deviations between calculated and observed intensities, and also anisotropies were calculated by Eqs. (17) and (18).

$$Dev_F(j) = \frac{F_{cal}(t_j) - F_{obs}(t_j)}{\sqrt{F_{cal}(t_j)}} \quad (17)$$

$$Dev_A(j) = \frac{A_{cal}(t_j) - A_{obs}(t_j)}{\sqrt{A_{cal}(t_j)}} \quad (18)$$

3. Results

3.1. Root of means square deviation (RMSD)

To evaluate the system stability, RMSDs of all-atoms relative to the corresponding starting structure coordinates of each system were calculated and plotted in Fig. S1 in Supporting Information (SI). The iBCC1 and iBCC2 denote to the first and second runs of MD calculations of cgGFP with ionic GYS, using BCC charges (see Method of MD calculation), and nBCC1 and nBCC2, MD runs of neutral GYS. The iRESP1, iRESP2 denote two runs of MD calculations with ionic GYS, and nRESP1 and nRESP2 with neutral GYS, using RESP charges. The RMSD values of all simulated systems rapidly increased during the first 10 ns as in the work by Teijeiro-Gonzalez et al. [20] and then fluctuated at ~2.0–2.5 Å throughout a simulation period of 100 ns. Based on the small fluctuation of the all-atom RMSDs, the equilibrated trajectory extracted from the last 40 ns (60–100 ns) were used for further analysis.

3.2. Inter-GYS distance

The inter-chromophore distance, $R(t')$, in a snapshot was obtained between mean coordinate of all aromatic atoms of GYSA and mean co-

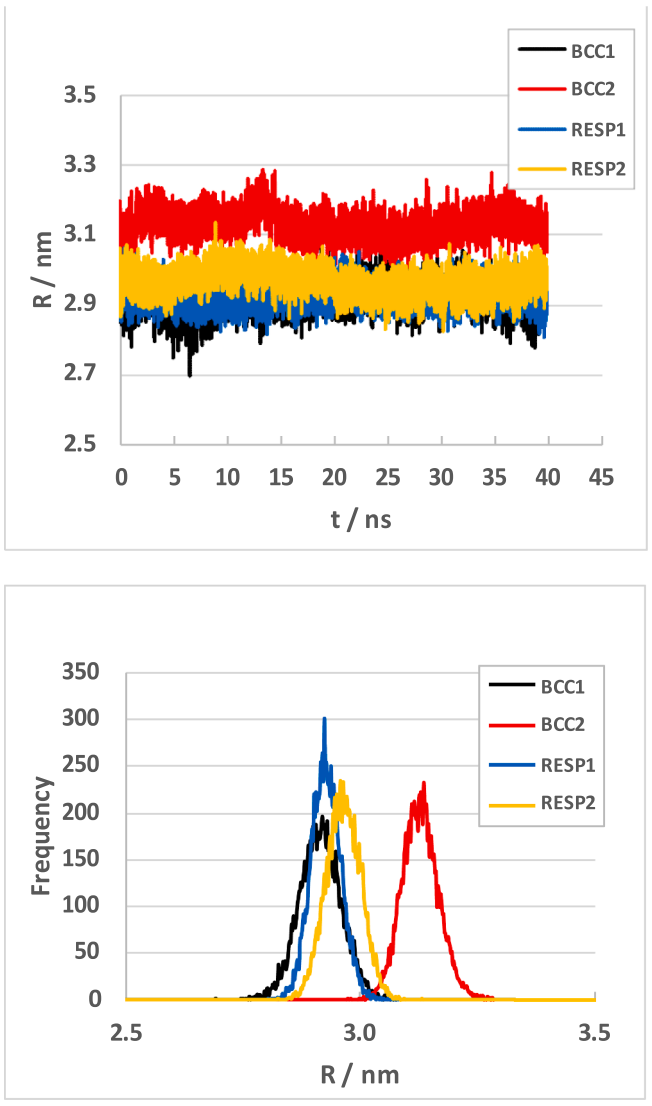

Fig. 2. Dynamics and distribution of inter-GYS distance with anionic GYS in cgGFP. Upper panel shows dynamics of the inter-chromophore distance, and lower panel distributions of the distances. BCC1 and BCC2 denote two independent runs of MD with BCC model, RESP1 and RESP2 with RESP models.

ordinate of all aromatic atoms of GYSB. Dynamics and distributions of $R(t')$ values with anionic GYS are shown in Fig. 2, in which proton of OH group in GYS is dissociated. The values of $R(t')$ in BCC2 displayed appreciably longer than the others. Maximum peaks of the distributions were around 2.9 nm in BCC1, RESP1 and RESP2, while it was 3.1 nm in BCC2. Dynamics and distributions of the $R(t')$ values in the neutral form are shown in Fig. 3. In the neutral cgGFP the $R(t')$ values displayed relatively steady with time in BCC1, BCC2 and RESP1. The $R(t')$ values were quite high in BCC1. The $R(t')$ value in RESP2 decreased with time. The peak values of $R(t')$ were around 2.9 nm in BCC2 and RESP1. In BCC1 run, the peak value was around 3.1 nm. In RESP2, the distribution displayed two maxima at around 3.05 and 3.15 nm.

Table 1 list the mean distances over 10,000 snapshots. The mean values (R) of $R(t')$ overall snapshots in anionic GYS were 2.9 and 3.1 nm with BCC1 and BCC2 models, and 2.9 and 3.0 nm in RESP1 and RESP2 models. The mean values of neutral GYS were 3.1 and 2.9 nm in BCC models, and 2.9 and 3.1 nm in RESP models. The R value did not seem to display appreciable difference between cgGFPs with anionic and neutral GYSs.

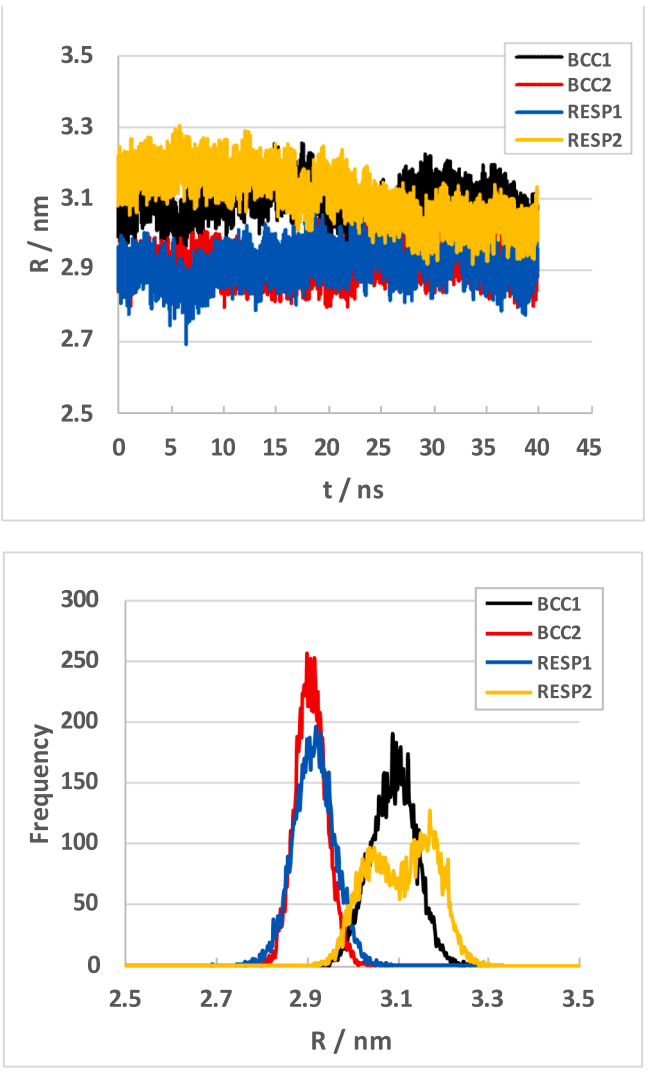

Fig. 3. Dynamics and distributions of inter-GYS distance with neutral GYS in cgGFP. Upper panel shows dynamics of the inter-chromophore distance, and lower panel distributions of the distances. BCC1 and BCC2 denote two independent runs of MD with BCC model, RESP1 and RESP2 with RESP models.

Table 1
Inter-GYS distance and inter-planar angle between two GYSs.[a]

MD run	Anion		Neutral	
	R / nm	Angle / deg	R / nm	Angle / deg
BCC1	2.9	46	3.1	87
BCC2	3.1	14	2.9	56
RESP1	2.9	39	2.9	46
RESP2	3.0	53	3.1	49
Mean[b]	2.98	38	3.00	60

[a] All aromatic atoms in GYSs are taken to calculate the distances and angles. Mean values were obtained over 10,000 snapshots with 4 ps intervals.
[b] The mean values over above four MD runs.

3.3. Inter-planar angle between two GYSs

A plane of GYS was obtained with three atomic coordinates of C1, CB2 and CZ in GYS (see Chart 1). The inter-planar angle at one snapshot was determined between the planes of GYSA and GYSB. Dynamics and distributions of inter-planar angles between two chromophores with anionic GYS are shown in Fig. 4. The angles displayed large variation with time from zero to almost 100 deg. The angles in BCC2 were

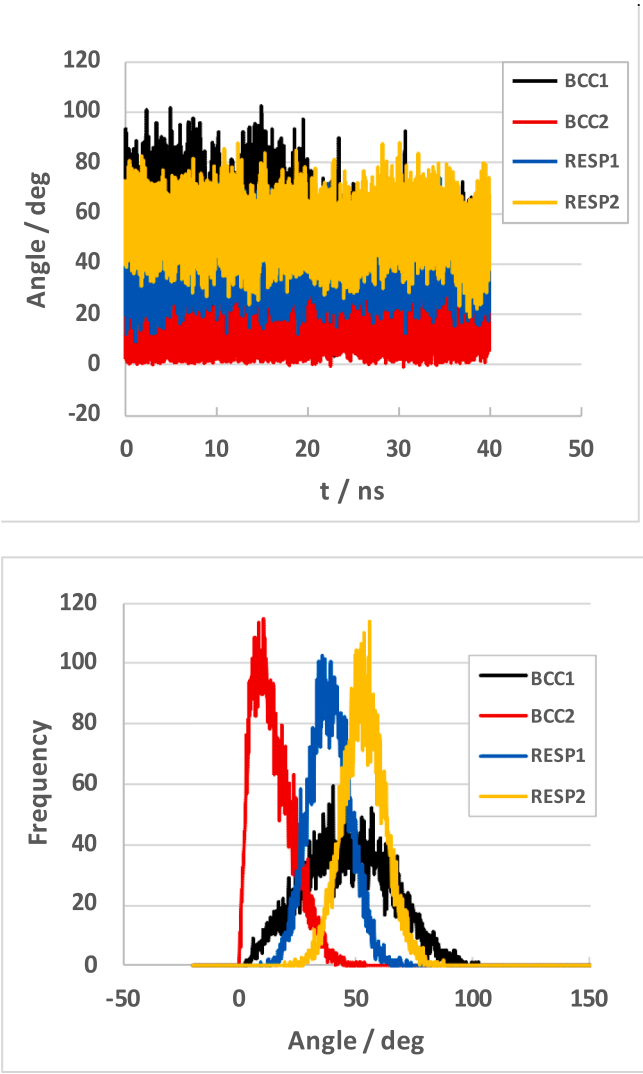

Fig. 4. Dynamics and distribution of inter-planar angle of anionic GYS in cgGFP. Upper panel shows inter-chromophore distance, and lower panel inter-planar angle. BCC1 and BCC2 denote two independent runs of MD with BCC model, RESP1 and RESP2 with RESP models.

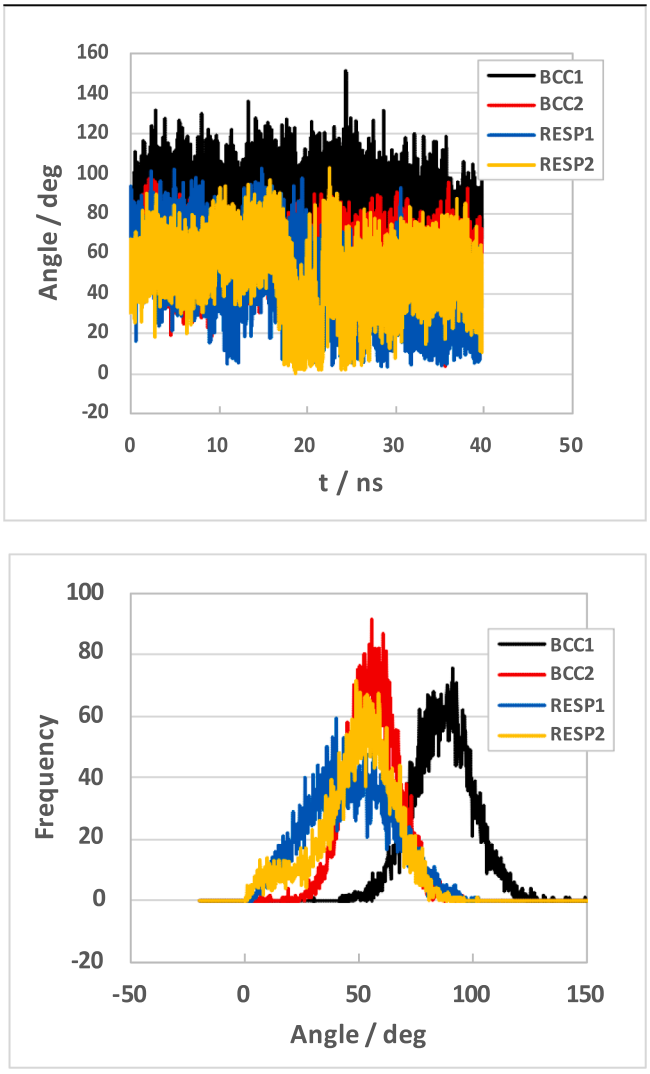

Fig. 5. Dynamics and distribution of inter-planar angle of neutral GYS in cgGFP. Upper panel shows inter-chromophore distance, and lower panel inter-planar angle. BCC1 and BCC2 denote two independent runs of MD with BCC model, RESP1 and RESP2 with RESP models.

relatively small, near to zero, while those in BCC1 and RESP2 were larger. The peak angles were around 10 deg in BCC2, 50 deg in both BCC1 and RESP1, and 60 deg in RESP2. The distribution displayed relatively sharp in BCC2, RESP1 and RESP2, while it was wider in BCC1. Mean angles of anionic cgGFP are listed in Table 1. The mean angles were 46 and 14 deg in BCC1 and BCC2, and 39 and 53 deg in RESP1 and RESP2. Mean angles over the four MD runs were listed at bottom line.

Fig. 5 shows dynamics and distributions of the inter-planar angles with neutral GYSs. The angle was largest in BCC1. The variation of the angles with time displayed a sudden change at around 20 ns in RESP2. The peak angle was around 80 deg in BCC1, 50 deg in BCC2 and RESP2, 40 deg in RESP1. The distributions were relatively sharp in BCC2 and RESP2 and were wider in RESP1. The mean angles in neutral GYSs are listed in Table 1. The angles were 87 and 56 deg in BCC1 and BCC2, and 46 and 49 deg in RESP1 and RESP2. The mean angles over four MD runs were 38 deg in anionic GYS and 60 deg in neutral GYS, which suggest that the inter-planar angle is quite high in neutral GYS than in anionic GYS.

Fig. 6 shows distributions of mean R and angle values. Here mean R and angle values denote the mean distance and angle over four MD runs at each MD time (10,000 snapshots with 4 ps intervals). The peak distributions were 2.98 nm in anionic cgGFP and 3.01 nm in neutral cgGFP. The distributions of the inter-planar angles were at around 37 deg in anionic cgGFP and 60 deg in neutral cgGFP.

3.4. Hydrogen bonding distance between atoms in GYS and nearby amino acids

Atom notations of GYS are shown in Chart 1. GYS contains N2, O2 and OH in aromatic ring, which are potential proton donors or acceptors upon HB formations with nearby amino acids. Snapshot of cgGFP with potential HBs between GYS and surrounding amino acids is illustrated in Fig. 1. The HBs between these heteroatoms in GYS and nearby amino acids could modify electronic state of the excited state. HB structures are good indicator for difference in the local structure around GYS between the two subunits. The HB distances (RHs) in crystal of cgGFP were 0.34 in GYS (O2) – Ser65 (peptide) pair, 0.29 in GYS (O2) – Gln95 (NE2), 0.28 in GYS (OH) – His149 (NE2), and 0.35 nm in GYS (OH) – Lys168 (NZ). These distances were the same in the two subunits in crystal. The RH values in solution obtained by MD methods are listed in Table 2. Formations of HB pairs are dependent on MD runs. In anionic cgGFP the HB pairs were GYS (O2) – Phe72 (peptide N), GYS (O2) – Tyr93 (OH), GYS (O2) – Gln95 (NE2) in Sub A, and GYS (O2) – Gln95 (NE2) in Sub B. The

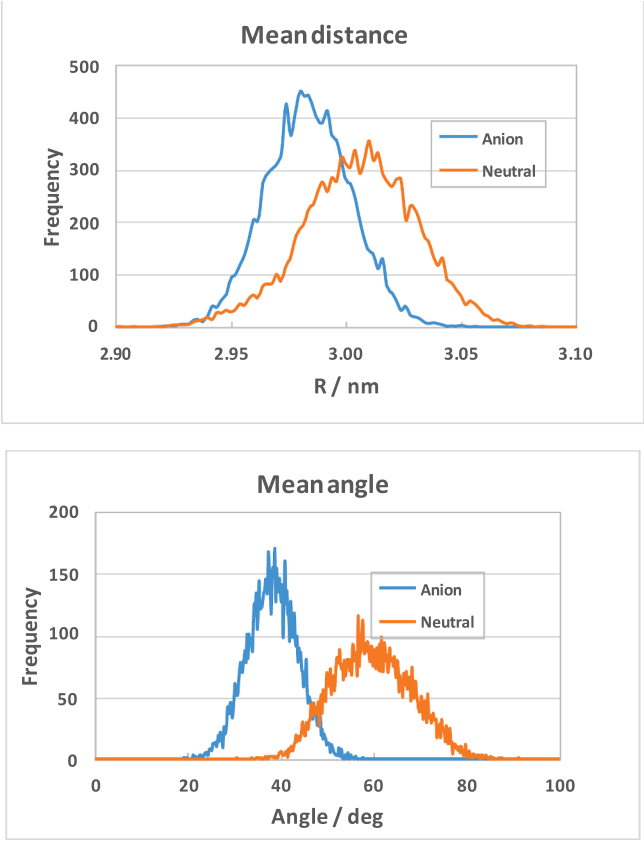

Fig. 6. Comparison of geometry between anionic and neutral cgGFPs. The distributions of R and angle values were obtained by taking averages over the four MD runs (BCC1, BCC2, RESP1 and RESP2) at each MD time.

phenolic O^- in anionic GYS forms HB with His149 (NE2) in Sub A, and Lys168 (NZ) in Sub B in BCC1. Thus five HBs formed in Sub A, and two in Sub B in BCC1 MD run. Atom notations of amino acids in parentheses were taken from PDB data. In anionic cgGFP in BCC2 run, the HB pairs were GYS(O2) – Gln95 (NE2) in Sub A and GYS(O2) – Gln95 (NE2) in Sub B, and GYS(O^-) – Lys168 (NZ) in Sub A. In BCC2 run, two HBs formed in Sub A, and one in Sub B. In RESP1 run, the HB pairs were GYS (O2) – Gln95 (NE2) both in Sub A and Sub B, and GYS (O^-) – Lys168 (NZ) both in Sub A and Sub B. The HB pairs in RESP2 run were similar with those in RESP1 run.

In neutral cgGFP with protonated OH group in GYS, the HB pairs in BCC1 run were GYS(O2) – Gln95 (NE2) in both Sub A and Sub B, GYS (OH) – His149 (ND1) in Sub B. Numbers of HB pairs were one in Sub A and two in Sub B. The HB pairs in BCC2 run were GYS (O2) – Gln95 (NE2) in both Sub A and Sub B. The HB pairs in RESP1 run were similar with those in BCC1 run, one in Sub A and two in Sub B. The HB pairs in RESP2 run were GYS(O2) – Gln95 (NE2) in both in Sub A and Sub B, GYS (O2) – Gln224 (OE1) in Sub B and GYS(OH) – Lys168 (NZ) in Sub B. Thus, numbers of HB pairs were one in Sub A and three in Sub B.

The HB pairs were dependent on BCC runs and RESP runs. However, the HB pair of GYS (O2) – Gln95 (NE2) appeared both in Sub A and Sub B, and both in anionic and neutral cgGFPs. The HB pair of GYS (O^-) – Lys168 (NZ) in anionic cgGFP was also common in all MD runs. In neutral cgGFP the HB pair of GYS (OH) – Lys168 (NZ) appeared only in RESP1 run, instead that HB pair of GYS (OH) – His149 (ND1) appeared in both BCC runs.

3.5. Distributions of RH

As stated above, the HB structure is a good indicator to see differences in the local structures between two subunits. The values of RH depend on the charge model (BCC or RESP) and MD runs. Here we took average of RH over all MD runs (two BCC and two RESP). The averaged RH distributions are compared between two subunits, in the pairs of GYS

Table 2
RH between heteroatoms of aromatic ring in GYS and nearby amino acids.[a]

GYS		BCC1			BCC2			RESP1			RESP2		
OH[b]	Atom	AA[c] (Atom)	Subunit	RH[d] (%[e])	AA[c] (Atom)	Subunit	RH[d] (%[e])	AA[c] (Atom)	Subunit	RH[d] (%[e])	AA[c]	Subunit	RH[d] (%[e])
Anion	O2	Phe72 (N)	A	0.28 (60)									
		Tyr93 (OH)	A	0.28 (58)									
		Gln95 (NE2)	A	0.30 (44)	Gln95 (NE2)	A	0.28 (99)	Gln95 (NE2)	A	0.28 (99)	Gln95 (NE2)	A	0.28 (99)
		Gln95 (NE2)	B	0.28 (91)	Gln95 (NE2)	B	0.29 (90)	Gln95 (NE2)	B	0.28 (99)	Gln95 (NE2)	B	0.31 (73)
	O^-	His149 (NE2)	A	0.28 (88)	Lys168 (NZ)	A	0.28 (96)	Lys168 (NZ)	A	0.27 (95)	Lys168 (NZ)	A	0.34 (100)
		Lys168 (NZ)	B	0.28 (96)				Lys168 (NZ)	B	0.27 (95)	Lys168 (NZ)	B	0.28 (96)
Neut-ral	O2	Gln95 (NE2)	A	0.29 (97)	Gln95 (NE2)	A	0.29 (64)	Gln95 (NE2)	A	0.29 (58)	Gln95 (NE2)	A	0.29 (99)
		Gln95 (NE2)	B	0.29 (99)	Gln95 (NE2)	B	0.29 (98)	Gln95 (NE2)	B	0.29 (83)	Gln95 (NE2)	B	0.29 (94)
											Glu224 (OE1)	B	0.28 (37)
	OH	His149 (ND1)	B	0.28 (93)				His149 (ND1)	B	0.29 (87)	Lys168 (NZ)	B	0.29 (48)

a Mean values over 10,000 snapshots with 0.004 ns intervals are listed. In crystal O2 of GYS forms HB with Ser65 (peptide O) with RH 0.34 nm, and with Gln95 (NE2) with RH 0.29 nm, and OH of GYS with His149 (CD2) with RH 0.28 nm.
b MD calculation were performed in the two ways, OH group of GYS is deprotonated, and neutral.
c Amino acid
d RH values are indicated in nm unit.
e Percentage occupation of HB.

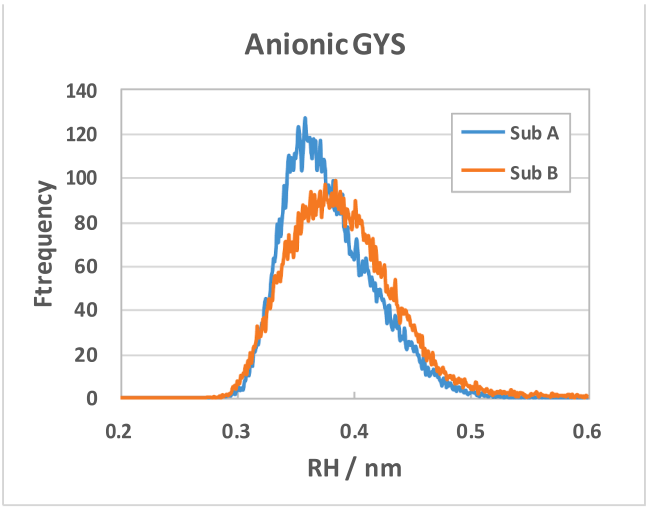

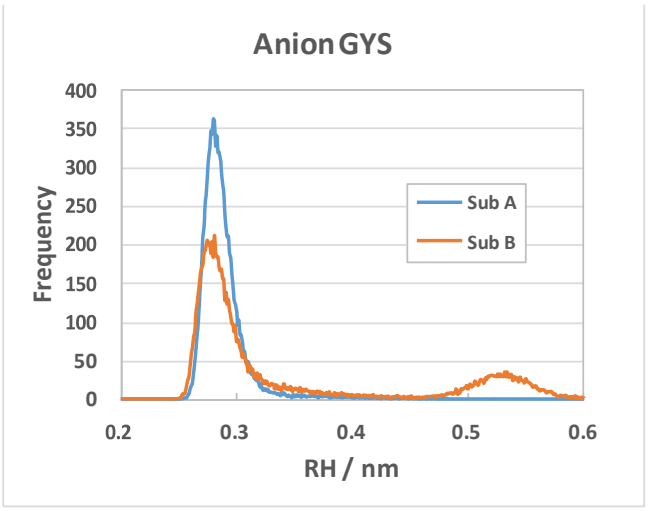

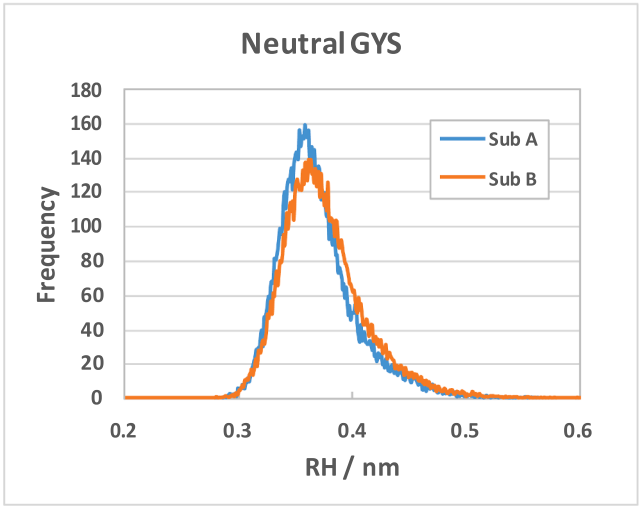

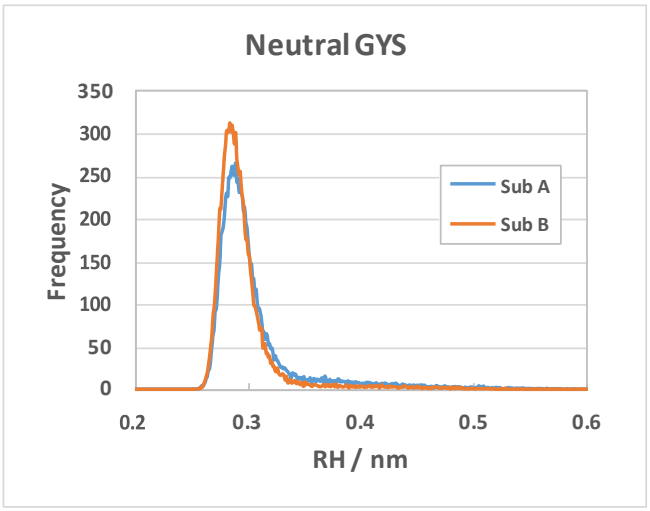

Fig. 7. Comparison of RH distributions between N2 of anionic or neutral GYS and Ser65O.

Fig. 8. Comparison of RH distributions between O2 of anionic or neutral GYS and Gln95NE1.

(O2) – Set65 (O), GYS (O2) – Gln95 (NE2) and GYS (OH) – Lys168 (NZ) both in anionic and neutral cgGFPs. In GYS (O2) – Ser65 pair no HB is formed in solution judging from mean RH value, but the HB is formed in crystal.

Fig. 7 compares the distributions of RH in GYS (O2) – Ser65 (O) pair between Sub A and Sub B in anionic and neutral cgGFPs, obtained as averaged values of the four MD runs. The peak RH values of anionic cgGFP were 0.36 nm in Sub A and 0.38 nm in Sub B. In neutral cgGFP, the peak RH values were both similar, 0.36 nm. Fig. 8 shows the RH distributions of GYS (O2) – Gln95 (NE2) pair. The peak RH values were both similar, 0.28 nm. In Sub B RH value displayed a second minor peak at around 0.54 nm. In neutral cgGFP the peak RH values were similar, 0.29 nm in Sub A and Sub B. The minor peak found in anionic cgGFP is not present in neutral cgGFP. Fig. 9 shows the RH distributions of GYS (O^-) – Lys168 (NZ) pair in anionic cgGFP and GYS (OH) – Lys168 (NZ) in neutral cgGFP. In anionic cgGFP, the RH values displayed sharp peaks at around 0.29 nm both in Sub A and Sub B. It displayed a minor peak at around 0.5 nm in Sub A, and at around 0.39 nm and 0.5 nm in Sub B. In neutral cgGFP, the distributions were much more complicated. Some of MD runs did not show HB in GYS (OH) – Lys168 (NZ) pair in neutral cgGFP (see Table 2). This may be the reason for the heterogeneous distribution. In Sub A, the main peak was at around 0.48 nm, the second peak at around 0.39 nm, and the third peak at around 0.29 nm. In Sub B, the main peak was at around 0.29 nm, the second peak at around 0.35 nm, and the third peak at around 0.5 nm. Only RESP2 run displayed HB in GYS (OH) – Lys168 (NZ) pair, and BCC1 and RESP1 runs did HB in GYS (OH) – His149 (ND1). These results reveal that HB structures near GYS chromophores are different between Sub A and Sub B. The anionic O^- of GYS seems to more strongly interact with Lys168 (NZ) with $-NH_3^{\pm}$ group than OH of GYS in the protein.

3.6. Dynamics and distributions of the square of orientation factor and related direct cosines in FRET rate

Fig. 10 shows dynamics of $cos\theta_T(t')$, $cos^2\theta_T(t')$, $cos\theta_A(t')$ and $cos\theta_B(t')$ in Eq. (6) (Top panel) and $\kappa^2(t')$ in Eq. (7) (middle panel) obtained by RESP1 run of MD calculation. Bottom panel of Fig. 10 shows distributions of these angles. The values of $cos\theta_T(t')$ decreased a little from −0.7 to −0.9 at 40 ns, and accordingly, the values of $cos^2\theta_T(t')$ increased with MD time. The values of $cos\theta_A(t')$ varied around −0.7, and those of $cos\theta_B(t')$ varied around −0.4, and sudden decrease a little in the time domain 15–20 ns. The values of $cos\theta_T(t')$ displayed a sharp peak at around −1.0 and a shoulder at around −0.8. The values of $cos^2\theta_T(t')$ also displayed a peak at around 1.0 and a minor peak at around 0.7. The values of $cos\theta_A(t')$ displayed a single peak at around 0.8. The values of $cos\theta_B(t')$ displayed two peaks, major at around −0.6 and minor at around −0.9. The values of $\kappa^2(t')$ decreased from ca. 0.7 at zero time to

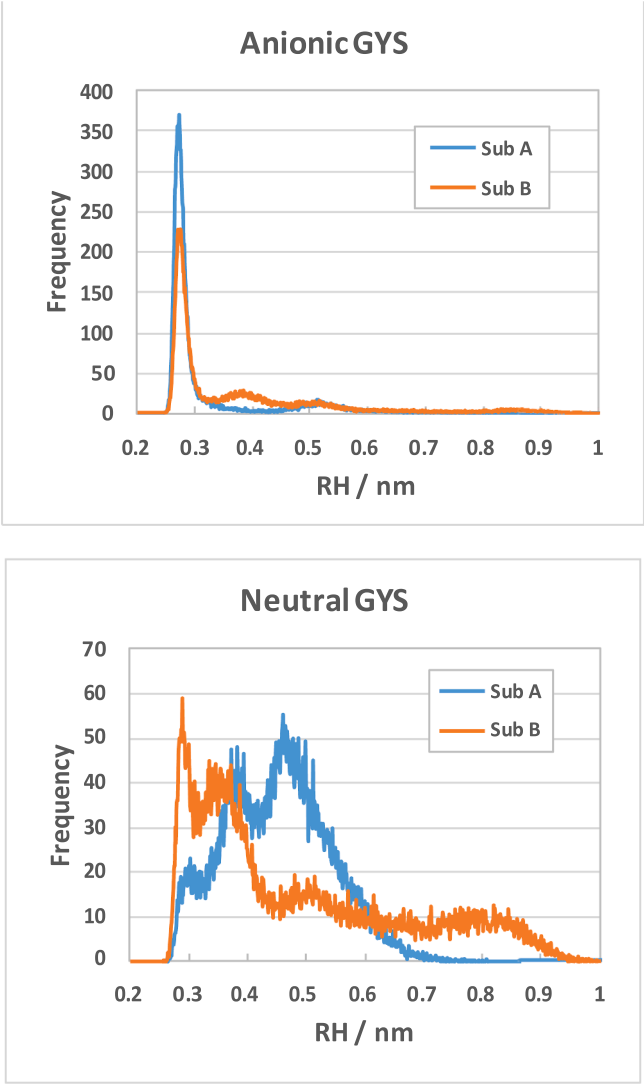

Fig. 9. Comparison of RH distributions between O^- of anionic GYS or OH of neutral GYS and Lys168NZ.

0.3 at 40 ns. It suddenly jumped from ca. 0.5 to *ca.* 1.2 at 15–20 ns. The sudden change in the $\kappa^2(t')$ values was due to sudden decrease in $cos\,\theta_B(t')$ in this time domain.

The MD time profiles of $cos\theta_T(t')$ and $\kappa^2(t')$ obtained with other runs, RESP2, BCC1, and BCC2 are shown in Fig. S2 (SI). The values of $cos^2\theta_T(t')$ in RESP2 run varied around 0.3 in 18 ns, and then suddenly increased to nearly 1, and decreased again to 0.6 in 40 ns. The values of $\kappa^2(t')$ in RESP2 run varied around 0.5 in 22 ns, and then increased to 1.0 in 40 ns. The values of $cos^2\theta_T(t')$ in BCC1 run decreased a little from 0.4 to 0.1 in 40 ns. The values of $\kappa^2(t')$ increased from 0.7 to 1.5 in the first 3 ns, and then further increased to 1.9 in 30–40 ns. The values of $cos^2\theta_T(t')$ in BCC2 run a little increased from 0.5 to 0.3 in 3 ns, then varied around 0.4 in 3–18 ns. The value suddenly decreased from 0.6 to 0.4 at 22 ns, then increased again from 0.4 to 0.6 in 35–40 ns. The values of $\kappa^2(t')$ in BCC2 run decreased from 1.3 to 0.5 in 18 ns, and then varied around 0.9.

3.7. *Dynamics and distributions of various rates related to FRET in cgGFP*

Fig. 11 shows dynamics and distributions of quenching rates due to HB formations between GYSs and nearby amino acids obtained by RESP1 run. Top panel of Fig. 11 shows time-dependent quenching rates due to HB between GYSA (RateA) given by Eq. (9) and GYSB (RateB)

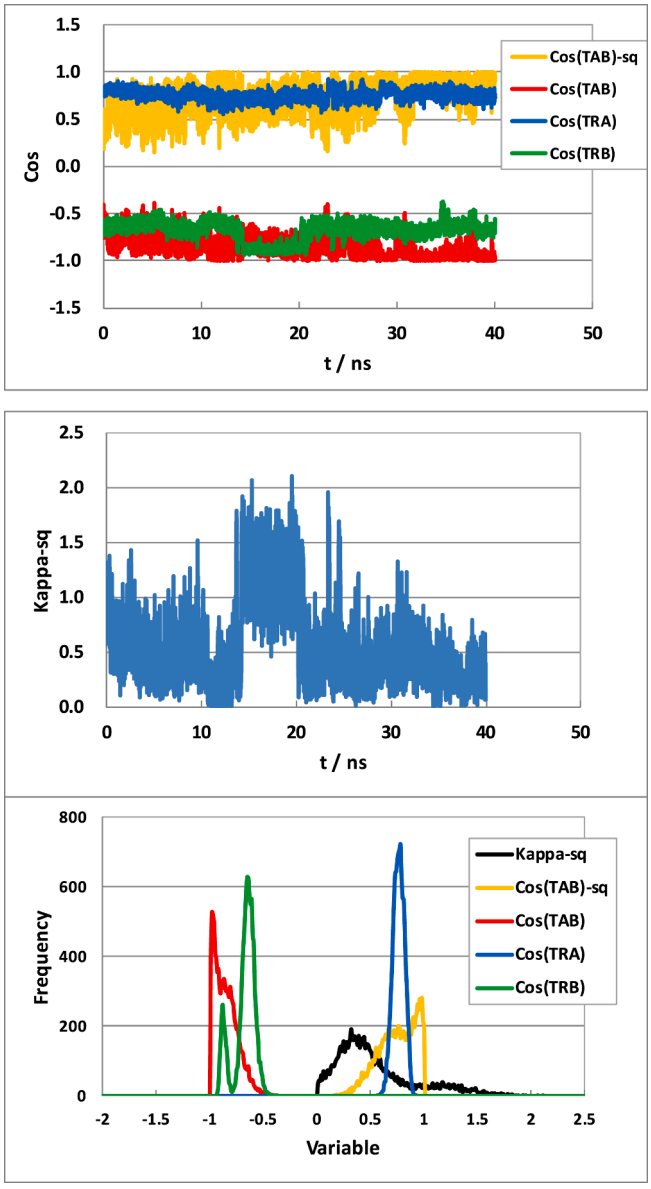

Fig. 10. Dynamics and distributions of square of orientation factor (Kappa) and related direct cosines. Cos(TAB) denotes direct cosine between transition moments of GYSA and GYSB [$cos\theta_T(t')$ in Eq. (6)]. Cos(TAB)-sq denotes $cos^2\theta_T(t')$. Cos(TRA) denotes direct cosine between distance vector connecting centers of GYSA and GYSB, and transition moment of GYSA [$cos\theta_A(t')$]. Cos(TRB) denotes direct cosine between the distance vector and transition moment of GYSB [$cos\theta_B(t')$]. Top panel shows dynamics of Cos(TAB), Cos(TRA) and Cos(TRB). The middle panel shows dynamics of Kappa-sq [Kappa given by Eq. (6)]. The bottom panel shows distributions of Cos(TAB), Cos(TRA), Cos(TRB), and Kappa-sq.

given by Eq. (10). The RateA varies around 0.28 ns^{-1} with MD time. The RateB decreased a little from 0.60 to 0.58 ns^{-1}in 40 ns. The quenching rates were quite different between Sub A and Sub B. Individual quenching rate is also shown in Fig. 11. The rate was highest in the HB pair, OH/His149NE1B in Sub B. In Sub A the HB formed only in the pair O2/Gln95NE2, and so the rates are identical with those of RATEA. Mean values of the quenching rates are listed in Table 3. Distributions of the RateA and RateB are shown in the middle panel. The distributions of the rates due to individual HB pair are shown in the bottom panel. Both distributions extended over wide range of the rates, though the rates at peak distributions are rather small around 0.5 ns^{-1} in FRETrateAB and around 1.2 ns^{-1} in FRETrateBA.

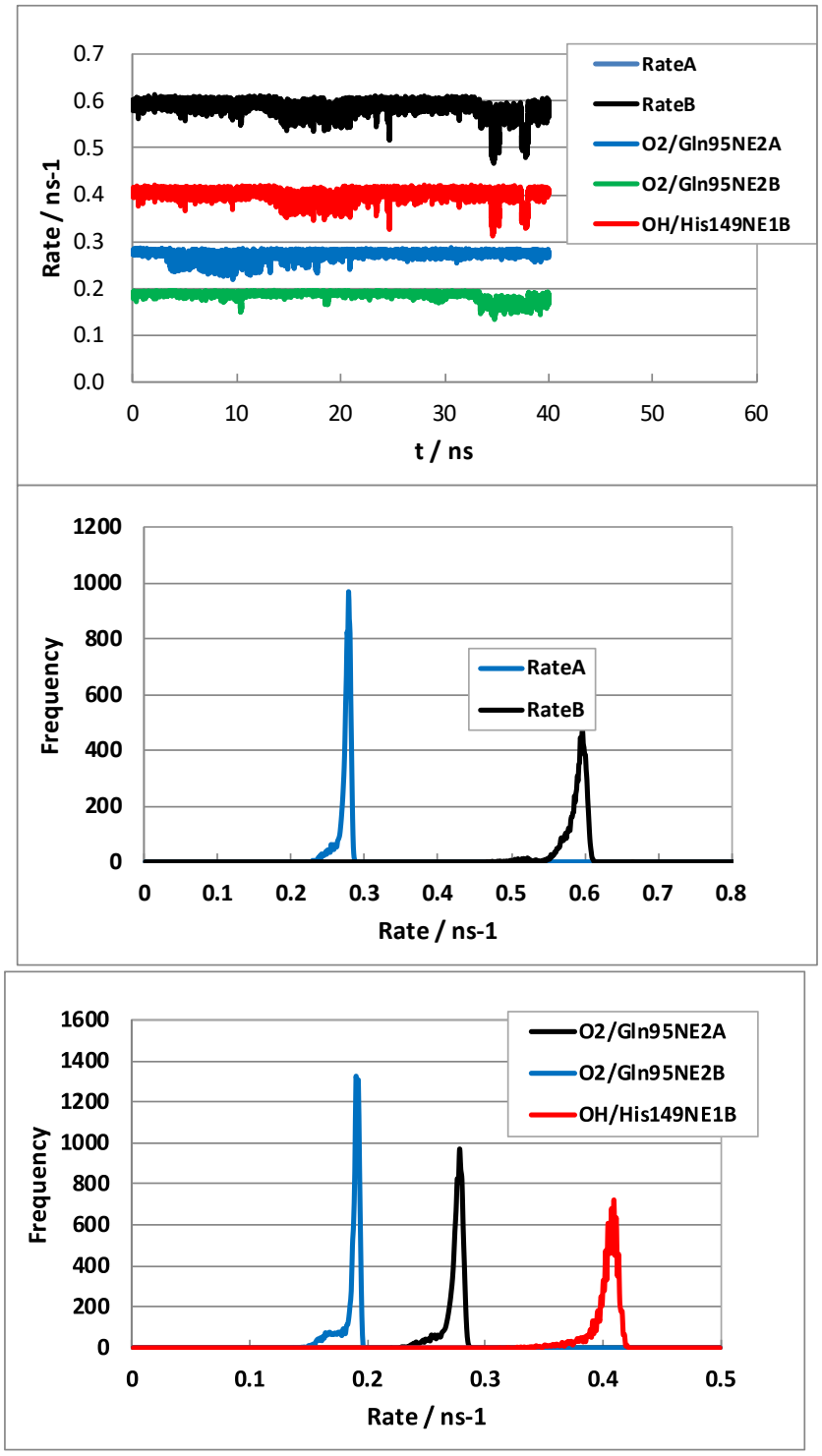

Fig. 11. Dynamics and distribution quenching rates due to HB formation between GYS nuclei and nearby amino acids. Top panel shows dynamics of quenching rates of k_A (t ') (RateA) obtained by Eq. (9) and of k_B (t ') (RateB) by Eq. (10). The rate due to individual HB pair is also shown. Second panel shows distributions of the quenching rates of RateA and RateB. Bottom panel shows distributions of the quenching rates due to HB pairs. See Table 3 for HB pairs.

Fig. 12 shows dynamics and distributions of FRETrates. Top panel shows time-dependent changes in the rates. The FRETrateAB from GYSA to GYSB given by Eq. (4) with RESP1 run markedly fluctuated. It decreased from *ca.* 2.5 ns^{-1} to 1 ns^{-1} in initial 14 ns, then jumped up to 4 ns^{-1} during 14–20 ns, then suddenly decreased to 1.5 ns^{-1} at 20 ns of MD time, followed by gradual decrease to 1 ns^{-1}at 40 ns. The MD time profile of FRETrateBA from GYSB to GYSB given by Eq. (5) was similar with that of FRETrateAB, though the values were a little lower than those of FRETrateAB. Distributions of the FRET rates are shown in the bottom panel. The MD time profiles of FRETrates were similar with that of $\kappa^2(t')$.

Figs. 10 and 12 suggest that the FRETrates are much influenced by $\kappa^2(t')$ rather than change in $R(t')$, because $\kappa^2(t')$ varies from zero to 1.5, while $R(t')$ varies in small range, though the rates depend on $R(t')$ with −6th power. The distribution of $\kappa^2(t')$ displayed two peaks, major and minor as stated above. This is ascribed to double peaks of Cos(TRB).

Table 3
Fluorescence quenching constants due to HB between GYS and nearby amino acids in cgGFP.[a]

MD run	GYS atom/Amino acid[b]	k^i_{QA} or k^i_{QB}	GYS atom/Amino acid[b]	k^i_{QA} or k^i_{QB}	GYS atom/Amino acid[b]	k^i_{QA} or k^i_{QB}	GYS atom/Amino acid[b]	k^i_{QA} or k^i_{QB}
RESP1	O2/Gln95 (NE2A)	0.37	O2/Gln95 (NE2B)	0.25	OH/His149 (NE1B)	0.54		
RESP2	O2/Gln95 (NE2A)	0.46	O2/Glu95 (OE1B)	0.13	O2/Glu224 (OE1B)	0.26	OH/Lys168 (NZB)	0.23
BCC1	O2/Gln95 (NE2A)	0.32	O2/Gln95 (NE2B)	0.27	OH/His149 (NE1B)	0.77		
BCC2	O2/Gln95 (NE2A)	0.41	O2/Gln95 (NE2B)	0.63				

a The mean quenching constants { k^i_{QA} in Eq. (9) for Sub A, and k^i_{QB} in Eq. (10) for Sub B} in unit of ns^{-1} over 10,000 MD snapshots with 4 ps intervals.
b Atom notations of GYS are indicated in Chart 1. The atoms notations of amino acids are taken from PDB file. Atoms of amino acids under HB interaction are shown in parentheses, together with subunit A or B.

Fig. 13 shows Lambda rates [λ_1 of Eq. (2) and λ_2 of Eq. (3)]. The values of Lambda2 display a similar time profile to FRETrateAB or FRETrateBA. The values were decreased from *ca.* 4 ns^{-1} to 2 ns^{-1} in initial 14 ns, then jumped to *ca.* 7 – 6 ns^{-1} from 14 to 20 ns. At 20 ns of MD time, it suddenly decreased to *ca.* 3 ns^{-1}, then further decreased a little to 2 ns^{-1} at 40 ns. The second panel of Fig. 13 shows the time-profile of Lambda1, which is expanded by 10 times in vertical axis. The profile of Lambda1 was quite different from that of Lambda 2. The values were initially varied around 0.37 ns^{-1} then decreased a little in 40 ns. The third panel shows distributions of Lambda1 and Lambda2. The values of Lambda2 distributed around 0.37 ns^{-1}, while those of Lambda1 (bottom panel) distributed in the range around 2 ns^{-1} and greater than 2 ns^{-1}.

The time-profiles of these rates obtained by RESP2 MD run are shown in Fig. S3 (SI). Top panel of Fig. S3 shows time-dependent quenching rates RateA and RateB. The values of RateA varies around 0.34 ns^{-1}. The RateB varied around 0.37 ns^{-1}up to *ca.* 20 ns, then around 3 ns^{-1}. The values of RateB were higher than those of RateA. The 2nd panel of Fig. S3 shows time-dependent changes in FRETrateAB and FRETrateBA. The values of FRETrateBA greatly varied between 0.1 and 2.5 ns^{-1} up to 22 ns, then increased with time to *ca.* 3 ns^{-1}. The time profile of FRETrateAB was similar with that of FRETrateBA. The 3rd panel of Fig. S3 shows time-profiles of Lambda1 and Lambda2. The values of Lambda2 were much larger than those of Lambda1 as in other runs. The bottom panel of Fig. S3 shows the time-profile Lambda1, in which vertical axis of the third penal was expanded. The values of Lambda1 varied between 0.34 and 0.36 ns^{-1}, while those of Lambda2 varied between 1 and 5 ns^{-1} up to 22 ns, and then increased with time to 2–8 ns^{-1}.

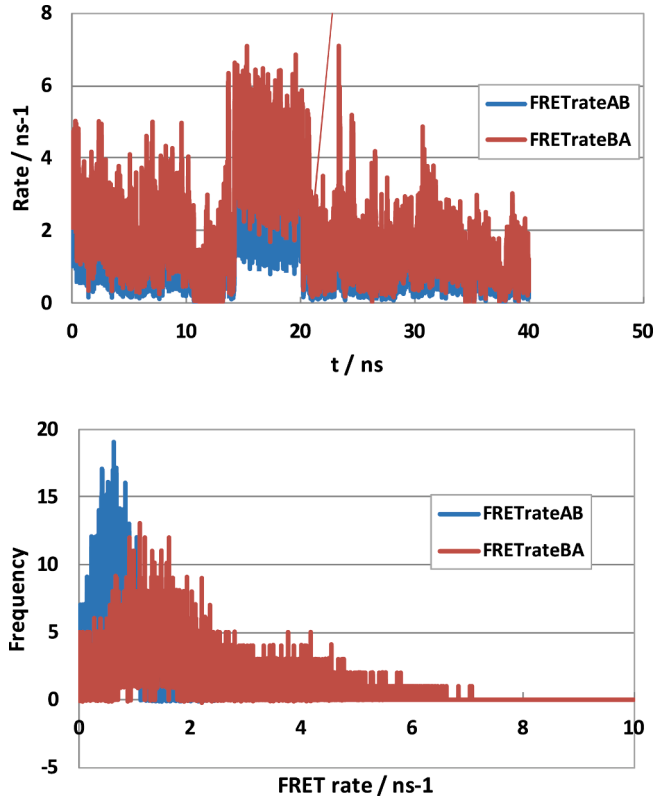

Fig. 12. Dynamics and distributions of FRETrates. Top panel shows FRETrateAB obtained by Eq. (4) and FRETrateBA obtained by Eq. (5). The lower panel shows distributions of the FRETrates.

The time-profiles of these rates obtained by BCC1 MD runs are shown in Fig S4 (SI). Top panel of Fig. S4 (SI) shows time-dependent quenching rates RateA and RateB. The RateA varies around 0.22 ns^{-1} and RateB around 0.79 ns^{-1}. The values of RateB were quite higher than those of RateA. The 2nd panel of Fig. S4 (SI) shows time-dependent changes in FRETrateAB and FRETrateBA. The values of both FRETrateAB and FRETrateBA varied around 3 ns^{-1} and 10 ns^{-1} with the MD time. The 3rd panel of Fig. S4 (SI) shows time-profiles of Lambda. The values of λ_2 were much greater than those of λ_1 as in RESP1 and RESP2 runs as described above. The bottom panel of Fig. S3 shows the time-profile of λ_1 expended in vertical axis of the 3rd panel. The values of λ_1 varied around 0.36 ns^{-1}.

The time-profiles of these rates obtained by BCC2 MD run are shown in Fig S5 (SI). Top panel of Fig. S5 shows time-dependent quenching rates of RateA and RateB. The values of RateA displayed sudden jumps at several MD times, as at 2 ns, 10, 26 and 33 ns. The values of RateB were quite stable and varied around 0.45 ns^{-1}. The 2nd panel of Fig. S5 (SI) shows time-dependent changes in FRETrateAB and FRETrateBA. The values of FRETrateAB varies between 2 and 8 ns^{-1}, while those of FRETrateBA between 4 and 10 ns^{-1}. The values of FRETrateAB were lower than those of FRETrateBA. The time profiles did not display sudden changes with MD time as in RESP1 run. The 3rd panel of Fig. S5 shows time-profiles of Lambda1 and Lambda2. The values of Lambda2 were much larger than those of Lambda1 as other MD runs. The bottom panel of Fig. S5 shows the time-profile of Lambda1 expanded in vertical axis of the 3rd panel. The values of Lambda1 varied around 0.32 – 0.37 ns^{-1}, while those of λ_2 varied between 5 and 15 ns^{-1}.

3.8. Mean quenching rates between GYS and nearby amino acids

The quenching constants, k^i_{QA} of GYSA and k^i_{QB} of GYSB for HB pair *i* due to HB formation between heteroatoms in GYS and nearby amino acids are listed in Table 3. In RESP1 run, the value of k^i_{QA} was 0.37 ns^{-1} due to HB between O2 atom in GYSA (see Chart 1 for atom notations of

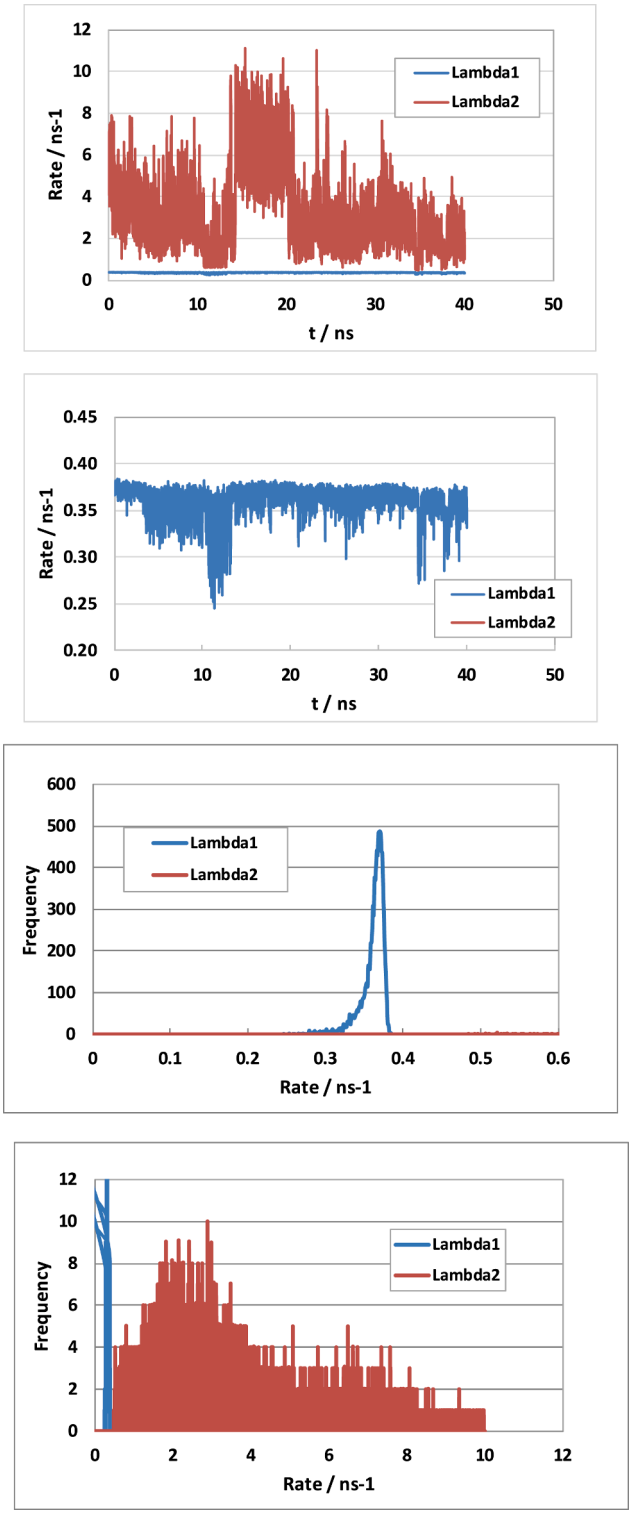

Fig. 13. Dynamics and distributions of Lambda rates Lambda1 rate are obtained by Eq. (2) and Lambda2 rate by Eq. (3). Top panel shows dynamics of Lambda1 and Lambda2. The vertical axis of Lambda1 was expended in the second panel. The third panel shows distributions of Lambda1 and Lambda2. The vertical axis of the third panel is expanded in the bottom panel.

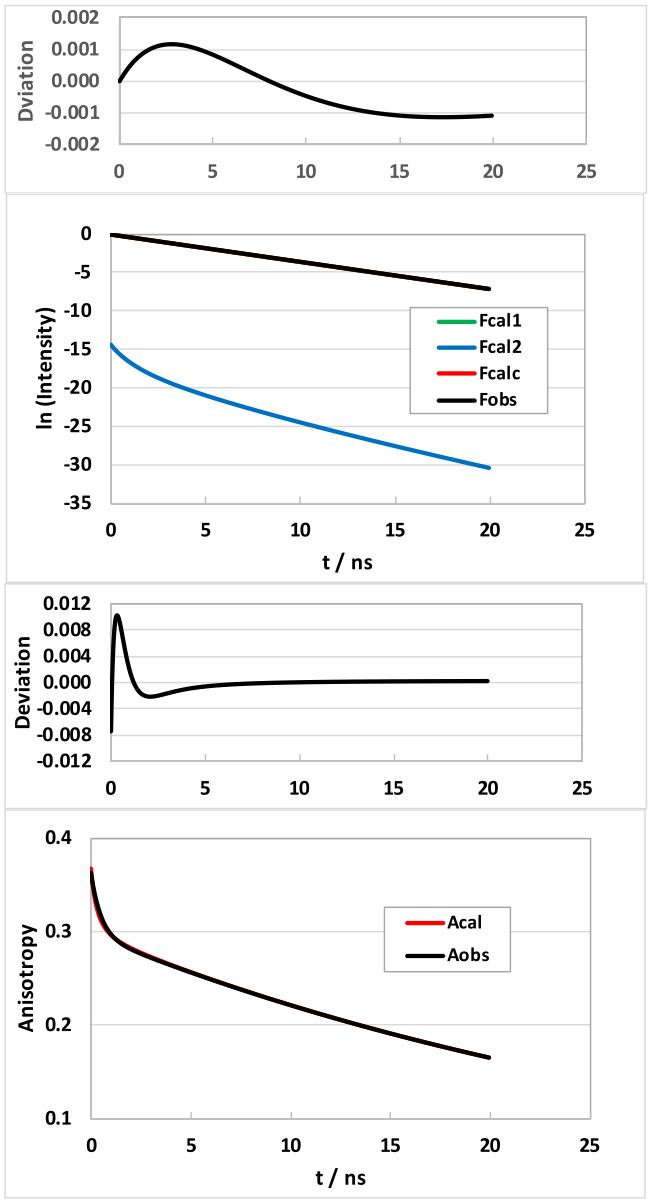

Figure 14. Observed and calculated decays of intensity and anisotropy in cgGFP with GYS in RESP1 run.The upper panels show the observed and calculated intensity decays obtained by Eqs (1) and (12), and their deviation obtained by Eq (17). The lower panels show the observed and calculated anisotropy decays obtained by Eqs (11) and (13), and their deviation obtained by Eq (18).

GYS) and Gln95NE2 (atom notations of amino acids were taken from PDB data). The values of k^i_{QB} were 0.25 ns^{-1} between O2 of GYSB and Gln95 (NE2), 0.54 between OH of GYSB and His149 (NE1).

In RESP2 run the values of k^i_{QA} were 0.46 ns^{-1} between O2 of GYSA and Gln95 (NE2). The values of k^i_{QB} were 0.13 between O2 and Gln95 (NE2), 0.26 between O2 of GYSB and Glu224 (OE1), 0.23 between OH of GYSB and Lys168 (NZ).

In BCC1 run, the value of k^i_{QA} was 0.32 ns^{-1} between O2 of GYSA and Gln95 (NE1). The values of k^i_{QB} were 0.27 ns^{-1} between O2 of GYSB and

Table 4
Physical c in cgGFP.[a]

MD run[b]	QAc (ns^{-1})	QBc (ns^{-1})	λ_1[d] (ns^{-1})	λ_2[d] (ns^{-1})	$cos^2\theta_T$[e]	κ^2[f]	R_e[g] (nm)	k_{AB}[h] (ns^{-1})	k_{BA}[h] (ns^{-1})	A_0i	Chi-F[j]	Chi-A[k]	Chi-total[l]
RESP1	0.27	0.59	0.36	3.23	0.74	0.53	3.93	0.87	1.87	0.37	7.9×10^{-7}	3.0×10^{-6}	1.9×10^{-6}
RESP2	0.34	0.38	0.36	3.82	0.47	0.62	4.33	1.64	1.83	0.48	1.4×10^{-7}	2.9×10^{-4}	1.4×10^{-4}
BCC1	0.24	0.78	0.36	13.0	0.16	1.41	4.42	2.90	9.47	0.80	2.5×10^{-8}	8.2×10^{-4}	4.1×10^{-4}
BCC2	0.29	0.47	0.36	10.6	0.43	0.71	4.49	3.94	6.27	0.80	5.8×10^{-7}	9.1×10^{-4}	4.6×10^{-4}

a The mean values were obtained over 10,000 snapshots (t') with 4 ps intervals.
b MD run with respect to atomic charges, and described in Ref 16.
c Mean value of $k_A(t')$ in Eq. (9) and $k_B(t')$ in Eq. (10) summed over HB pairs.
d Coupled rates interacting by FRET between GYSA and GYSB, given by Eqs. (2) and (3).
e $cos^2\theta_T$ in Eq. (11)
f $\kappa^2(t')$ in Eq. (7).
g Reduced critical transfer distance given by Eqs. (7) and (8).
h Mean values of FRET rates, k_{AB} given by Eq. (4), and k_{BA} given by Eq. (5).
i Normalization factor for anisotropy in Eq. (11).
j Chi-square of the intensity given by Eq. (15).
k Chi-square of the anisotropy given by Eq. (16).
l Total chi-square given by Eq. (14).

Glu95 (NE1), 0.77 ns^{-1} between OH of GYSB and His149 (NE1). In BCC2 run, the value of k^i_{QA} was 0.41 ns^{-1} between O2 of GYSA and Gln95 (NE1). The value of k^i_{QB} was 0.63 ns^{-1} between O2 of GYSB and Gln95 (NE1).

3.9. Calculated intensity and anisotropy decays of GYSs obtained with RESP1 run

Fig. 14 shows the observed and calculated fluorescence intensity and anisotropy decays. Top panels of Fig. 14 show the fluorescence intensity decay and its deviation between the observed and calculated intensities given by Eq. (17). The observed intensity decay [18] is,

$$F_{obs}(t) = exp(-t/2.78) \quad (19)$$

$F_{cal}(t)$ was obtained by Eq. (12). F_{cal1} in insert of Fig. 14 denote $F_{cal1}(t) = \langle F_1 exp\{\lambda_1(t')t\}\rangle_{AV}$ in Eqs. (1) and (12). It is evident from Fig. 14 that $F_{cal2}(t)$ was much less than $F_{cal1}(t)$, which shows $F_{cal1}(t)$ is responsible for the observed decay of $F_{cal}(t)$ in Eq. (12), which implies that the calculate intensity decay is single exponential with the rate of $\lambda_1(t')$ as experimental decay [18]. The obtained lifetime, $1/\lambda_1(t')$ was 2.70 ns, which is close to the observed lifetime, 2.78 ns [18]. Agreements between the observed and calculated intensities were excellent as shown in the deviations between the decays.

The bottom panel of Fig. 14 shows the observed and calculated anisotropy decays. The observed decay is represented as Eq. (20) [18].

$$A_{obs}(t) = \{0.034exp(-t/0.51) + 0.339\}exp(-t/34) \quad (20)$$

A_{cal} in Fig. 14 is given by Eq. (13). The deviations between the observed and calculated anisotropy decays are given by Eq. (18). Agreement between the calculated and experimental anisotropy decays were also excellent.

The observed and calculated fluorescence intensity and anisotropy are shown in Fig. S6 (SI) decays obtained by RESP2 run, in Fig. S7 obtained by BCC1 run, and in Fig. S8 obtained by BCC2 run.

3.10. Physical quantities related to intensity and anisotropy decays in cgGFP obtained with the four MD runs

Table 4 lists various physical quantities related to FRET and chi-squares with four MD runs. The values of F_1 in Eq. (1) were 1.0 in all MD runs, while those of F_2 were negligible. The mean quenching rates of $k_A(t')$ in Eq. (9) and $k_B(t')$ in Eq. (10) over 10,000 snapshots are represented by Q_A and Q_B, respectively. The values of Q_A and Q_B were 0.27 and 0.59 ns^{-1} with RESP1 run, 0.34 and 0.38 ns^{-1} with RESP2 run, 0.24 and 0.78 ns^{-1} with BCC1 run, and 0.29 and 0.47 ns^{-1} with BCC2 run. The values of the coupling rates by FRET interaction, λ_1 and λ_2, were 0.36 and 3.23 ns^{-1} by RESP1, 0.36 and 3.82 ns^{-1} by RESP2, 0.36 and 13.0 ns^{-1} by BCC1 and 0.36 and 10.6 ns^{-1} by BCC2 run. Mean values of $cos^2\theta_T(t')$ in Eq. (11) were 0.74 by RESP1, 0.47 by RESP2, 0.16 by BCC1 and 0.43 by BCC2. Mean values of square of orientation factor given by Eq. (7) were 0.53 by RESP1, 0.62 by RESP2, 1.41 by BCC1 and 0.71 by BCC2. The values of R_e in Eqs. (4) and (5) were 3.93 with RESP1, 4.33 with RESP2, 4.42 by BCC1 and 4.49 by BCC2 run. Experimental value of R_e is 4.26 [18]. Mean values of FRET rate from GYSA to GYSB, k_{AB} given by Eq. (4) and k_{BA} given by Eq. (5) were 0.87 and 1.87 ns^{-1} with RESP1, 1.64 and 1.83 ns^{-1} with RESP2, 2.90 and 9.47 ns^{-1} with BCC1, and 3.94 and 6.27 ns^{-1} with BCC2 run. The values of A_0 were 0.37 with RESP1, 0.48 by RESP2, 0.80 by BCC1, and 0.80 by BCC2 run. Theoretical value of A_0 is 0.4, and experimental value, 0.373 [18].

The values of Chi-F, Chi-A and Chi-total, given by Eqs. (15), (16) and (14) were 7.9×10^{-7}, 3.0×10^{-6} and 1.9×10^{-7} with RESP1, 1.4×10^{-7}, 2.9×10^{-4} and 1.4×10^{-4} with RESP2, 2.5×10^{-8}, 8.2×10^{-4}, 4.1×10^{-4} by BCC1, 5.8×10^{-7}, 9.1×10^{-4} and 4.6×10^{-4} with BCC2 run. Thus, RESP1 run was best among the four MD runs, considering the values of Chi-total and A_0.

4. Discussion

Structural differences in the entire cgGFP proteins between anionic and neutral forms were studied by observing inter-GYS distances and inter-planar angles, using MD structures in solution. MD calculations were performed with two kinds of atomic charges of the protein, BCC and RESP models, and with two independent runs for each model. Conformational differences between anionic and neutral cgGFPs, and between the two subunits were judged from mean values of the distances and angles among the four MD runs.

The inter-planar angle displayed appreciable difference between anionic and neutral cgGFPs, while the inter-GYS distance did not. The differences in the local structures between the two subunits and between the anionic and neutral cgGFPs were examined through HB structures between aromatic heteroatoms of GYS and nearby amino acids. The GYS (O2) – Gln95 (NE2) pair seemed to form quite strong HB both in anionic and neutral cgGFPs, and both in Sub A and Sub B, and also in crystal. HB formation in GYS (O^-) or GYS (OH) and Lys168 or His149 (NE2) was dependent on the MD run, though GYS (OH) formed HB with both Lys168 and His149 in crystal. Presumably, His149 and Lys168 compete for HB formation with GYS (O^-) or GYS (OH) in solution. Large difference in the HB structures between Sub A and Sub B were found in GYS (O^-) or GYS (OH) – Lys168 (NZ) pair. The non-equivalent HB structures

are also found between isoalloxazine and nearby amino acids in many flavoproteins [42–45].

FRET phenomenon in neutral cgGFP dimer was analyzed with theoretical expressions with the atomic coordinates obtained by four independent MD runs with two RESP models and two BCC models. Agreements between the experimental intensity and anisotropy decays and the calculated decays were best with RESP1 run, and then RESP2 run, which suggests that RESP model is better than BCC model in the present study. The agreements between the experimental and calculated intensity decays were very good with any MD runs, but those of the anisotropy decays were highly dependent on the MD model.

Fraction with lifetime of $\tau_1 = 1.40$ ns increases as concentration of cgGFP is lowered [18], which reveals that lifetime of the monomer is 1.4 ns, while that of dimer is 2.78 ns. Microenvironment surrounding GYS in the monomer is considered to be modified upon the dimer formation as in many flavoproteins [42–45]. It is noted that the dimer displays single lifetime, even though the quenching rates without FRET interaction are different between Sub A and Sub B. When the both GYSs interact by FRET, the observed lifetimes become $1/\lambda_1$ and $1/\lambda_2$. In cgGFP fraction of intensity decay with lifetimes of 1 $/\lambda_2$ is negligible. Theoretical expressions of the intensity and anisotropy decays used in the present study [25] are derived assuming FRET donor and acceptor are fixed. In cgGFT both GYSs are fixed in the protein at certain snapshot at MD time t'.

The calculated intensity and anisotropy decays were obtained by taking average over all MD snapshots. In Eq. (1) the values of F_2 were all nearly zero in any MD runs, while those of F_1 were nearly 1.00, which are in agreement with the experimental decay [18]. In the previous study [18] FRETrate was evaluated assuming $k_{AB}(t') = k_{BA}(t')$. This assumption is valid when the environments around GYSA and GYSB are equivalent. As stated above, the pair of HB formation and number of the pair are not the same between Sub A and Sub B. Actually the values of Q_A and Q_B were quite different (0.27 ns^{-1} and 0.59 ns^{-1} with RESP1 run, see Table 4). The OH group of GYS was assumed to be neutral in cgGFP.

Dynamic behavior of various rates and geometrical factors were greatly dependent on the MD models and even on MD runs with the same model. The values of $\kappa^2(t')$ displayed sudden jump around 15–20 ns of MD time with RESP1 run. The sudden jump in FRETrateAB and FRETrateBA are ascribed to the jump in $\kappa^2(t')$. This should be due to dynamic conformational change in the protein structures of Sub A and Sub B of cgGFP in this period.

The model compound analogous to GYS free from the protein displays absorption peak at around 370 nm in ethanol, while it becomes at 430 nm upon adding NaOH [46]. This longer absorption band is due to phenolate, O^- of the model compound. Both species are non-fluorescent at room temperature. As solvent viscosity increases, both species become fluorescent, which suggests that the torsional motion between the two aromatic rings is responsible for the fast internal conversion. Fluorescence lifetimes were 0.6 ps (99.9 %) and 0.32 ns (0.1 %) in ethanol at 275 K, while they are 0.8 ps (94.5 %) and 4.2 ps (5.5 %) upon adding NaOH [46]. According to molecular orbital calculations, rotational motion takes place around CB2-CA2 bond (see Chart 1) in the excited state of the free chromophore [47].

Photophysics of cgGFT is not known yet as in avGFT. The cgGFT displays absorption peaks at 485 nm which is in visible range, and the emission peak at 500 nm [10], while those are 380 and 480 nm in avGFP, respectively [48]. The HB structures play an important role on the photophysics of avGFP. Behavior of excited state of avGFP is quite complicated. The absorbance at around 380 nm decreases upon illumination at 400 nm for several hours, and instead the absorbance at around 480 nm increases [48]. Photophysics of avGFP was studied by method of two-photon excitation [48]. Excited state of A1* converts to A2* by a conformational change (CC), and then proton of OH group in phenol part of GYS transfers to nearby water molecule (ESPT) to form state I*. Absorption of I state displays at around 490 nm, and emission at around 590 nm. State B is different from A1 or A2 state which displays absorption band at around 470 nm and emission band at around 509 nm. Fluorescence lifetimes of I* and B* are identified to be 3.3 and 2.8 ns. The phenolate O^- in GYS in avGFP mutant S65T/H148D forms very strong HB with Asp148 (RH = 0.245 nm), resulting in significant spectral perturbations [48]. The pKa value of the phenolate was modified incorporating halogen atoms into phenol nucleus. Absorption spectrum of avGFP remarkably shifted toward longer wavelength with reducing the pKa value. In cgGFP, the HB pairs between OH of GYSB and His149 (NE1) in Sub B, and between O2 and Gln95 (NE1) both in Sub A and Sub B were most effective for the fluorescence quenching, as stated above.

Anisotropy decay in YFP abnormally displayed negative values at very early stage of time [19]. The negative anisotropy could occur when angle between transition moments of absorption and emission is larger than 62 deg. The negative anisotropy is considered to be as a result of unidirectional FRET from the donor chromophore in the neutral form to the acceptor chromophore in the anionic form in the YFP dimer [19]. The negative anisotropy was theoretically predicted in a bichromophoric system in protein, where FRET donor and acceptor possess motional freedom with special arrangement of the mutual transition moments [49,50]. Teijeiro-Gonzalez et al have theoretically analyzed their precise experimental anisotropy with two models, 1) the anisotropy is expressed by a stretched exponential decay model, and 2) the anisotropy is expressed as sum of independent exponential terms of rotational motion of EGFP and of FRET. It is noted that contributions of rotational motion and FRET to depolarization is expressed as products of the two terms [18,50–53]. Mancini et al. [54] have examined aggregation state of beta amyloid protein by means of time-dependent fluorescence anisotropies of Tyr in the proteins. They analyzed the anisotropy data with Monte Carlo method and MD method.

To our knowledge three methods to analyze experimental anisotropy decay under FRET interactions have been proposed, 1) theoretical expressions obtained by rotational diffusion equation [50–53], 2) autocorrelation functional method, originally proposed by Ichie and Karplus [21], and Henry and Hochstrasser [22] and 3) the present method. The expressions were always very complicated when the problem was solved with rotational diffusion equations [50–53]. Even autocorrelational method is used for the anisotropy analyses under FRET interactions, it is required to postulate analytical model as in the work by Teijeiro-Gonzalez et al. [20]. It is not straightforward to connect the obtained correlation time with molecular structure of the fluorophore. Physical picture of present method is clear, and obtained quantities are directly connected to the protein structure.

CRediT authorship contribution statement

Nadtanet Nunthaboot: Conceptualization, Methodology, Software, Data curation, Writing- original draft preparation, Reviewing and Editing the final version. **Fumio Tanaka:** Conceptualization, Methodology, Software, Data curation, Writing- original draft preparation, Reviewing and Editing the final version. **Jan W. Borst:** Supervision, Writing – review & editing. **Antonie J.W.G. Visser:** Conceptualization, Methodology.

Declaration of Competing Interest

The authors declare that they have no known competing financial interests or personal relationships that could have appeared to influence the work reported in this paper.

Acknowledgements

This work was motivated by AJWG Visser. He passed away on 28 October 2018 during his preparation of the present manuscript. We would like to dedicate this work to his memory. N. N. gratefully acknowledged the Center of Excellence for Innovation in Chemistry (PERCH-CIC), Ministry of Higher Education, Science, Research and Innovation. The Structural and Computational Biology Research Unit (Chulalongkorn University) is acknowledged for computational facilities.

Appendix A. Supplementary data

Supplementary data to this article can be found online at https://doi.org/10.1016/j.jphotochem.2021.113584.

References

[1] O. Shimomura, F.H. Johnson, Y. Saiga, Extraction, purification and properties of aequorin, a bioluminescent protein from the luminous hydromedusan, Aequorea. J. Cell. Comp. Physiol. 59 (1962) 223–239.
[2] O. Shimomura, . The discovery of green-fluorescent protein. In Green-Fluorescent Protein (Chalfie, M., and Kain, S., (Eds.), pp 3–15, Wiley-Liss, New York, 1998.
[3] R.Y. Tsien, The green fluorescent protein, Ann. Rev. Biochem. 67 (1998) 509–544.
[4] O.V. Stepanenko, V.V. Verkhusha, I.M. Kuznetsova, V.N. Uversky, K.K. Turoverov, Fluorescent proteins as biomarkers and biosensors: Throwing color lights on molecular and cellular processes, Curr. Prot. Pep. Sci. 9 (2008) 338–369.
[5] M. Ormö, A.B. Cubitt, K. Kallio, L.A. Gross, R.Y. Tsien, S.J. Remington, Crystal structure of the Aequorea victoria green fluorescent protein, Science 273 (1996) 1392–1395.
[6] F. Yang, L.G. Moss, G.N. Phillips, The molecular structure of green fluorescent protein, Nat. Biotechnol. 14 (10) (1996) 1246–1251.
[7] M. Chattoraj, B.A. King, G.U. Bublitz, S.G. Boxer, Ultra-fast excited state dynamics in green fluorescent protein: multiple states and proton transfer, Proc. Natl. Acad. Sci. USA 93 (16) (1996) 8362–8367.
[8] H. Lossau, A. Kummer, R. Heinecke, F. Pöllinger-Dammer, C. Kompa, G. Bieser, T. Jonsson, C.M. Silva, M.M. Yang, D.C. Youvan, M.E. Michel-Beyerle, Time-resolved spectroscopy of wild-type and mutant green fluorescent proteins reveals excited state deprotonation consistent with fluorophore-protein interactions, Chem. Phys. 213 (1-3) (1996) 1–16.
[9] M.A. Lill, V. Helms, Proton shuttle in green fluorescent protein studied by dynamic simulations, Proc. Nat. Acad. Sci. USA 99 (5) (2002) 2778–2781.
[10] S.S. Patnaik, S. Trohalaki, R. Pachter, Molecular modeling of green fluorescent protein: structural effects of chromophore deprotonation, Biopolymers 75 (6) (2004) 441–452.
[11] R. Nifosì, V. Tozzini, Molecular dynamics simulations of enhanced green fluorescent proteins: effects of F64L, S65T and T203Y mutations on the ground-state proton equilibria, Proteins 51 (3) (2003) 378–389.
[12] S.S. Patnaik, S. Trohalaki, R.R. Naik, M.O. Stone, R. Pachter, Computational study of the absorption spectra of green fluorescent protein mutants, Biopolymer 85 (3) (2007) 253–263.
[13] E.Y. Lau, J.L. Phillips, M.E. Colvin, Computational study of the absorption spectra of green fluorescent protein mutants, Mol. Phys. 107 (2009) 1233–1241.
[14] C.M. Megley, L.A. Dickson, S.L. Maddalo, J. Gabriel, G.J. Chandler, M. Zimmer, Photophysics and dihedral freedom of the chromophore in yellow, blue, and green fluorescent protein, J. Phys. Chem. B 113 (2009) 302–308.
[15] L.D. Levine, W.W. Ward, Isolation and characterization of a photoprotein, "phialidin", and a spectrally unique green-fluorescent protein from the bioluminescent jellyfish *Phialidium gregarium*, Comp. Biochem. Physiol. 72 (1) (1982) 77–85.
[16] S.V. Markova, L.P. Burakova, L.A. Frank, S. Golz, K.A. Korostileva, E.S. Vysotski, Green-fluorescent protein from the bioluminescent jellyfish *Clytia gregaria*: cDNA cloning, expression, and characterization of novel recombinant protein, Photochem. Photobiol. Sci. 9 (2010) 757–765.
[17] M.S. Titushin, Y. Feng, G.A. Stepanyuk, Y. Li, S.V. Markova, S. Golz, B.C. Wang, J. Lee, J. Wang, E.S. Vysotski, Z.J. Liu, NMR-derived topology of a GFP-photoprotein energy transfer complex, J. Biol. Chem. 285 (2010) 40891–40900.
[18] N.P. Malikova, N.V. Visser, A. van Hoek, V.V. Skakun, E.S. Vysotski, J. Lee, A.J.W. G. Visser, Green-fluorescent protein from the bioluminescent jellyfish clytia gregaria. Is an obligate dimer and does not form a stable complex with the Ca^{2+}-discharged photoprotein clytin, Biochemistry 50 (20) (2011) 4232–4241.
[19] X. Shi, J. Basran, H.E. Seward, W. Childs, C.R. Bagshaw, S.G. Boxer, Anomalous negative fluorescence anisotropy in yellow fluorescent protein (YFP 10C): Quantitative analysis of FRET in YFP Dimers, Biochemistry 46 (2007) 14403–14417.
[20] Y. Teijeiro-Gonzalez, A. Crnjar, A.J. Beavil, R.L. Beavil, J. Nedbal, A. Le Marois, C. Molteni, K. Suhling, Time-resolved fluorescence anisotropy and molecular dynamics analysis of a novel GFP homoFRET dimer, Biophys. J. 120 (2) (2021) 254–269.
[21] T. Ichiye, M. Karplus, Fluorescence depolarization of tryptophan residues in proteins: a molecular dynamics study, Biochemistry 22 (12) (1983) 2884–2893.
[22] E.R. Henry, R.M. Hochstrasser, Molecular dynamics simulations of fluorescence polarization of tryptophans in myoglobin, Proc. Nat. Acad. Sci. USA 84 (17) (1987) 6142–6146.
[23] N. Nunthaboot, F. Tanaka, S. Kokpol, N.V. Visser, H. van Amerongen, A.J.W. G. Visser, Molecular dynamics simulation of energy migration between tryptophan residues in apoflavodoxin, RSC Adv. 4 (2014) 31443–31451.
[24] N.V. Visser, A.H. Westphal, A. van Hoek, C.P. van Mierlo, A.J. Visser, H. van Amerongen, (2008) Tryptophan-tryptophan energy migration as a tool to follow apoflavodoxin folding, Biophys. J. 95 (2008) 2462–2469.
[25] Tanaka, F. and Mataga, N. (1979) Theory of time-dependent photo-selection in interacting fixed systems. Photochem. Photobiol. 29, 1091–1098.
[26] Frisch, M.J., Schlegel, H. B., Scuseria, G. E., Robb, M. A., Cheeseman, J. R., Scalmani, G., Barone, V., Mennucci, B., Petersson, G. A., Nakatsuji, H, Caricato, H., Li, X., Hratchian, H.P., Izmaylov, A. F., Bloino, J., Zheng, G., Sonnenberg, J. L., Hada, M., Ehara, M., Toyota, K., Fukuda, R., Hasegawa, J., Ishida, M., Nakajima, T., Honda, Y., Kitao, O., Nakai, H., Vreven, T., Montgomery Jr., J. A., Peralta, J. E., Ogliaro, F., Bearpark, M. J., Heyd, J., Brothers, E. N., Kudin, K. N., Staroverov, V. N., Kobayashi, R., Normand, J., Raghavachari, K., Rendell, A. P., Burant, J. C., Iyengar, S. S., Tomasi, J., Cossi, M., Rega, N., Millam, N. J., Klene, K., Knox, J. E., Cross, J. B., Bakken, V., Adamo, C., Jaramillo, J., Gomperts, R., Stratmann, R. E., Yazyev, A Ö., Austin, J., Cammi, R., Pomelli, C., Ochterski, J. W., Martin, R. L., Morokuma, K., Zakrzewski, V. G., Voth, G. A., Salvador, P., Dannenberg, J. J., Dapprich, S., Daniels, A. D., Farkas, O., Foresman, J. B., Ortiz, J. V., Cioslowski, J., Fox, D. J., Gaussian 09. Gaussian, Inc. 2009.
[27] C.I. Bayly, P. Cieplak, W. Cornell, P.A. Kollman, A well-behaved electrostatic potential based method using charge restraints for deriving atomic charges: the RESP model, J. Phys. Chem. 97 (1993) 10269–10280.
[28] J. Wang, R.M. Wolf, J.W. Caldwell, P.A. Kollman, D.A. Case, Development and testing of a general amber force field, J. Comput. Chem. 25 (2004) 1157–1174.
[29] J.A. Maier, C. Martinez, K. Kasavajhala, L. Wickstrom, K.E. Hauser, C. Simmerling, ff14SB: improving the accuracy of protein side chain and backbone parameters from ff99SB, J Chem Theory Comput. 11 (8) (2015) 3696–3713.
[30] Case, D. A., Darden, T. A., Cheatham, T. E., Simmerling, C. L., Wang, J., Duke, R. E., Luo, R., Walker, R. C., Zhang, W., Merz, K. M., Roberts, B., Hayik, S., Roitberg, A., Seabra, G., Swails, J., Goetz, A. W., Kolossváry, I., Wong, K. F., Paesani, F., Vanicek, J., Wolf , R. M., Liu, J., Wu, X., Brozell, S. R., Steinbrecher, T., Gohlke, H., Cai, Q., Ye, X., Wang, J., Hsieh, M. J., Cui, G., Roe, D. R., Mathews, D. H., Seetin, M. G., Salomon-Ferrer, R., Sagui, C., Babin, V., Luchko, Gusarov, T. S., Kovalenko, A., Kollman, P. A., AMBER 14 University of California, San Francisco. 2014.
[31] W.L. Jorgensen, J. Chandrasekhar, J.D. Madura, R.W. Impey, M.L. Klein, Comparison of simple potential functions for simulating liquid water, J. Chem. Phys. 79 (1983) 926–935.
[32] B.A. Luty, W.F. van Gunsteren, Calculating electrostatic interactions using the particle−particle particle−mesh method with nonperiodic long-range interactions, J. Phys. Chem. 100 (1996) 2581–2587.
[33] J.-P. Ryckaert, G. Ciccotti, H.J.C. Berendsen, Numerical integration of the Cartesian equations of motion of a system with constraints: Molecular dynamics of n-alkanes, J. Comput. Phys. 23 (3) (1977) 327–341.
[34] Th. Förster, Fluoreszenz Organischer Verbindungen, Vandenhoek and Ruprecht, Gottingen, 1951.
[35] L. Stryer, Fluorescence energy transfer as a spectroscopic ruler, Ann. Rev. Biochem. 47 (1978) 819–846.
[36] B.W. VanDerMeer, Kappaphobia is the elephant in the fret room, Methods Appl. Fluoresc. 8 (3) (2020) 030401, https://doi.org/10.1088/2050-6120/ab8f87.
[37] J. Herbrich, J. Waluk, R.P. Thummel, C.Y. Hung, Mechanisms of fluorescence quenching by hydrogen bonding in various aza aromatics, J. Photochem. Photobiol. A 80 (1994) 157–160.
[38] A. Cser, K. Nagy, L. Biczok, Fluorescence lifetime of Nile Red as a probe for the hydrogen bonding strength with its microenvironment, Chem Phys. Lett. 360 (2002) 473–478.
[39] A.K. Singh, S. Das, A. Karmakar, A. Kumar, A. Datta, Solvation and hydrogen bonding aided efficient non-radiative deactivation of polar excited state of 5-aminoquinoline, Phys. Chem. Chem. Phys. 20 (2018) 22320–22330.
[40] I. Bhattacharjee, N. Ghosh, J. Dasgupta, D. Ray, Conformational switching *via* an intramolecular H-bond modulates the fluorescence lifetime in a novel coumarin–imidazole conjugate, Phys. Chem. Chem. Phys. 20 (2018) 6060–6072.

[41] S. Xie, S. Manugri, O. Ramström, M. Yan, Impact of hydrogen bonding on the fluorescence of *N*-amidinated fluoroquinolones, Chem. Asian J. 14 (2019) 910–916.
[42] H. Chosrowjan, S. Taniguchi, T. Wongnate, J. Sucharitakul, P. Chaiyen, F. Tanaka, Conformational heterogeneity in pyranose 2-oxidase from Trametes multicolor revealed by ultrafast fluorescence dynamics, J. Photochem. Photobiol. A 234 (2012) 44–48.
[43] N. Nunthaboot, K. Lugsanangarm, A. Nueangaudom, S. Pianwanit, S. Kokpol, F. Tanaka, S. Taniguchi, H. Chosrowjan, T. Nakanishi, M. Kitamura, Photoinduced electron transfer from aromatic amino acids to the excited isoalloxazine in flavin mononucleotide binding protein. Is the rate in the inverted region of donor – acceptor distance not real? J. Photochem. Photobiol. A 326 (2016) 60–68.
[44] K. Lugsanangarm, A. Nueangaudom, S. Kokpol, S. Pianwanit, N. Nunthaboot, F. Tanaka, S. Taniguchi, H. Chosrowjan, Heterogeneous subunit structures in the pyranose 2-oxidase homotetramer revealed by theoretical analysis of the rates of photoinduced electron transfer from a tryptophan to the excited flavin, J. Photochem. Photobiol. A 306 (2015) 66–79.
[45] A. Nueangaudom, K. Lugsanangarm, S. Pianwanit, S. Kokpol, N. Nunthaboot, F. Tanaka, Phys. Chem. Chem. Phys. 14 (2012) 2567–2578.
[46] A.D. Kummer, C. Kompa, H. Niwa, T. Hirano, S. Kojima, M.E. Michel-Beyerle, Viscosity-dependent fluorescence decay of the GFP chromophore in solution due to fast Internal conversion, J. Phys. Chem. B 106 (2002) 7554–7559.
[47] C. Jiang, A. Fang, D. Zhao, H. Li, R. Xie, F. Li, Detailed photoisomerization dynamics of a green fluorescent protein chromophore based molecular switch, Int. J. Photoenergy 2014 (2014), 597165.
[48] G. Striker, V. Subramaniam, C.A.M. Seidel, A. Volkmer, Photochromicity and fluorescence lifetimes of green fluorescent protein, J. Phys. Chem. B 103 (1999) 8612–8617.
[49] L.M. Oltrogge, S.G. Boxer, Short hydrogen bonds and proton delocalization in green fluorescent protein (GFP), ACS Cent. Sci. 1 (2015) 148–156.
[50] F. Tanaka, Theory of time-resolved fluorescence under the interaction of energy transfer in a bichromophoric system: effect of internal rotations of energy donor and acceptor, J. Chem. Phys. 109 (3) (1998) 1084–1092.
[51] F. Tanaka, Effects of internal rotations on the time-resolved fluorescence in a bichromophoric protein system under the energy transfer interaction, J. Fluorescence 10 (2000) 13–20.
[52] P.I. Bastiaens, A. van Hoek, J.A. Benen, J.C. Brochon, A.J. Visser, Conformational dynamics and intersubunit energy transfer in wild-type and mutant lipoamide dehydrogenase from Azotobacter vinelandii. A multidimensional time-resolved polarized fluorescence study, Biophys. J. 63 (3) (1992) 839–853.
[53] J.J. Fisz, Polarized fluorescence spectroscopy of two-ground- and two-excited-state systems in solutions, Chem. Phys. Lett. 262 (1996) 495–506.
[54] O. Mancini, T. Wellbrock, O.J. Rolinski, K. Kubiak-Ossowska, P.A. Mulheran, Probing beta amyloid aggregation using fluorescence anisotropy: experiments and simulation, Phys. Chem. Chem. Phys. 20 (2018) 4216–4225.